A POD-based reduced order method applied to Goda time-splitting scheme

Mejdi Azaiez, Tomas Chacon Rebollo, Fernandez Nunez, Samuel Rubino

A POD-based reduced order method applied to Goda time-splitting scheme

M. Azaïez[*], T. Chacón Rebollo [†], C. Núñez Fernández [‡], S. Rubino [§]

November 29, 2024

Abstract

This paper presents a first-order approximation for solving the unsteady Stokes problem using the pressure-correction Goda scheme in the Reduced Order Model (ROM) context. The study begins by formulating a semi-discrete in time approximation of the Stokes problem, followed by the introduction of the Goda time-splitting scheme, employing the first-order Euler approximation for time discretization. A brief overview of the Finite Element (FE) space approximation is also provided. The Proper Orthogonal Decomposition (POD) method is then used to construct a Galerkin projection-based ROM for the Goda equations. An interesting point of the present contribution lies in the choice of inner products used to construct reduced bases for predicted velocities, divergence-free velocities, and pressure. These choices lead to explicit calculations for deriving velocity and pressure solutions within the reduced model. Stability analysis and error estimates for the proposed ROM are derived. Finally, numerical examples are presented to validate the theoretical results, demonstrating the effectiveness and accuracy of the proposed approach also for the simulation of the parametrized incompressible Navier–Stokes equations.

Keywords: Navier–Stokes equations, Time-splitting schemes, Proper orthogonal decomposition, Reduced order methods, Incompressible flows, Numerical analysis.

[*]Bordeaux University, Bordeaux INP and I2M (UMR CNRS 5295), France. azaiez@u-bordeaux.fr

[†]Departamento EDAN & IMUS, Universidad de Sevilla, Spain. chacon@us.es

[‡]Virtualmechanics, S.L. & IMUS, Universidad de Sevilla, Spain. c.nunez@virtualmech.com

[§]Departamento EDAN & IMUS, Universidad de Sevilla, Spain. samuele@us.es

1 Introduction

A significant challenge in the numerical simulation of incompressible flows arises from the coupling between velocity and pressure, imposed by the incompressibility constraint. Interest in using projection methods to address this issue in time-dependent viscous incompressible flows began in the late 1960s, with the pioneering work of Chorin and Temam [8, 42]. Since then, various extensions of these methods, commonly referred to as fractional or splitting step methods, have been developed. The literature on this subject is extensive, featuring both rigorous mathematical analysis and a wide array of numerical experiments. For a detailed treatment of this topic, see [36, 19].

It is important to note that projection methods provide an efficient alternative to un-split methods, which often rely on techniques such as Uzawa algorithms, known for their high computational cost. For more details on these alternative approaches, see [37, 42, 16]. The key advantage of projection methods lies in their ability to decouple the velocity and pressure equations at each time step, requiring the solution of a series of independent elliptic/parabolic equations. This makes them particularly well-suited for large-scale numerical simulations [21].

This motivates the study of projection methods within the framework of reduced-order methods. Another significant advantage of these methods is that the issue of pressure recovery, often encountered in non-splitting approaches, is effectively eliminated. Indeed, if the reduced velocity basis weakly satisfies the incompressibility constraint, the contribution of the pressure, which is precisely the Lagrange multiplier in the equations ensuring the constraint, formally drops out from the Reduced Order Model (ROM). On this subject, one can see for example [1, 33, 3, 41, 4, 34, 7]. In projection methods, the pressure is directly computed by solving a ROM that depends on the predicted velocity, which is not divergence-free. This streamlined process further enhances the efficiency and simplicity of the method.

As far as we know from the bibliography, very little work has been published on the study and analysis of reduced-order methods using time-splitting techniques to solve unsteady Stokes and/or incompressible Navier–Stokes problems. In this respect, we can cite the work of Li et al. [32] where they proposed and studied a Proper Orthogonal Decomposition based Reduced-Order Model (POD-ROM) for non-stationary Stokes equations, which combines the classical Chorin–Temam projection method with POD technique. The method decouples the reduced-order velocity variable and reduced-order pressure variable. They circumvent the verification of classical LBB/inf-sup condition for mixed reduced spaces with the help of pressure stabilized Petrov–Galerkin (PSPG)-type projection method. In this contribution, we propose a reduced order method applied to the time-splitting Goda (standard-incremental) scheme [17], which constitutes an improvement over the classical Chorin–Temam pressure-correction scheme. We choose to compute

the pressure POD modes using a scalar product offering the double advantage of being consistent with the regularity of the pressure in the full order Finite Element (FE) resolution and leading to a completely explicit calculation for both reduced velocity and pressure.

The outline of the paper is listed as follows. In Section 2, we recall the unsteady Stokes problem and give its semi-discrete in time approximation. Then, we present the Goda time-splitting scheme using the first order-Euler approximation for time discretization, and we briefly describe its FE space approximation. In Section 3, we mainly introduce POD method and construct a Galerkin ROM for the Goda equations. In Section 4, we perform the stability and error analysis of the proposed ROM. In Section 5, some numerical examples are conducted to validate the theoretical analysis, and demonstrate the effectiveness and accuracy of the proposed approach also for the simulation of the parametrized incompressible Navier–Stokes equations. Finally, Section 6 presents the main conclusions of this work and ongoing research directions.

2 Time-dependent Stokes equations and Goda time-splitting scheme

We consider the incompressible evolution Stokes Equations (SE) given by:

$$\begin{cases} \boldsymbol{u}_t - \nu\Delta\boldsymbol{u} + \nabla p &= \boldsymbol{f} \qquad \text{in } \Omega\times(0,T), \\ \nabla\cdot\boldsymbol{u} &= 0 \qquad \text{in } \Omega\times(0,T), \\ \boldsymbol{u} &= \boldsymbol{0} \qquad \text{on } \partial\Omega, \\ \boldsymbol{u}(x,0) &= \boldsymbol{u}_0(x) \qquad \text{in } \Omega, \end{cases} \tag{1}$$

in a bounded polyhedral domain $\Omega \subset \mathbb{R}^d$, $d \in \{2,3\}$, with a Lipschitz-continuous boundary $\partial\Omega$, and in the time interval $[0,T]$. For the sake of simplicity, we impose homogeneous Dirichlet boundary conditions on $\partial\Omega$.

In the above equations (1), $\boldsymbol{u}$ is the velocity field, p is the pressure of the incompressible fluid, $\nu > 0$ is the kinematic viscosity, $\boldsymbol{f}$ is the forcing term, and $\boldsymbol{u}_0$ is the initial velocity.

2.1 Goda time-splitting scheme

We describe the time discretization of the unsetady Stokes problem (1) used in this work.

Time discretization. In order to specify the time discretization, let us divide the time interval of integration $[0,T]$ into N subdivisions of length $\Delta t = T/N$,

the time step, and define $t^n = n\Delta t$, $0 \leq n \leq N$. We shall compute two sequences $(\boldsymbol{u}^n)_{0\leq n\leq N}$ and $(p^n)_{0\leq n\leq N}$ in a recurrent way that approximate in some sense $(\boldsymbol{u}(\cdot,t^n))_{0\leq n\leq N}$ and $(p(\cdot,t^n))_{0\leq n\leq N}$. Assuming $(\boldsymbol{u}^k,p^k)_{0\leq k\leq n}$ to be known, we then determine $\boldsymbol{u}^{n+1}$ and p^{n+1} by solving:

$$\left\{\begin{array}{rll} \dfrac{\boldsymbol{u}^{n+1}-\boldsymbol{u}^n}{\Delta t} - \nu\Delta\boldsymbol{u}^{n+1} + \nabla p^{n+1} &= \boldsymbol{f}^{n+1} & \text{in } \Omega, \\ \nabla\cdot\boldsymbol{u}^{n+1} &= 0 & \text{in } \Omega, \\ \boldsymbol{u}^{n+1} &= \boldsymbol{0} & \text{on } \partial\Omega, \end{array}\right. \tag{2}$$

where, for simplicity of presentation, we have considered the first order Euler time scheme.

The Goda time-splitting scheme [17] adopted here acts into 2 steps. The first is the prediction-diffusion problem that consists in:

Find $\tilde{\boldsymbol{u}}^{n+1}$ *such that*

$$\left\{\begin{array}{rll} \dfrac{\tilde{\boldsymbol{u}}^{n+1}-\boldsymbol{u}^n}{\Delta t} - \nu\Delta\tilde{\boldsymbol{u}}^{n+1} + \nabla p^{n} &= \boldsymbol{f}^{n+1} & \text{in } \Omega, \\ \tilde{\boldsymbol{u}}^{n+1} &= \boldsymbol{0} & \text{on } \partial\Omega. \end{array}\right. \tag{3}$$

The second step, called pressure-continuity correction step, consists in:

Find $(\boldsymbol{u}^{n+1},\phi^{n+1})$ *such that*

$$\left\{\begin{array}{rll} \dfrac{1}{\Delta t}(\boldsymbol{u}^{n+1}-\tilde{\boldsymbol{u}}^{n+1}) + \nabla\phi^{n+1} &= \boldsymbol{0} & \text{in } \Omega, \\ \nabla\cdot\boldsymbol{u}^{n+1} &= 0 & \text{in } \Omega, \\ \boldsymbol{u}^{n+1}\cdot\boldsymbol{n} &= 0 & \text{on } \partial\Omega, \end{array}\right. \tag{4}$$

with $\boldsymbol{n}$ the unit normal to $\partial\Omega$ oriented outward. This last step can be rewritten as a Poisson problem on ϕ^{n+1} :

Find ϕ^{n+1} *such that:*

$$\left\{\begin{array}{rll} \Delta\phi^{n+1} &= \dfrac{1}{\Delta t}\nabla\cdot\tilde{\boldsymbol{u}}^{n+1} & \text{in } \Omega, \\ \\ \partial_{\boldsymbol{n}}\phi^{n+1} &= 0 & \text{on } \partial\Omega. \end{array}\right. \tag{5}$$

Finally, the divergence-free corrected velocity and the pressure are computed by:

Find $\boldsymbol{u}^{n+1}$ *and* p^{n+1} *such that:*

$$\begin{array}{rcl} \boldsymbol{u}^{n+1} &=& \tilde{\boldsymbol{u}}^{n+1} - \Delta t\nabla\phi^{n+1} \text{ in } \Omega, \\ p^{n+1} &=& p^n + \phi^{n+1} \text{ in } \Omega. \end{array} \tag{6}$$

In order to give a variational formulation of the time-splitting method (3)-(6), let us introduce the predicted velocity space:

$$\tilde{\boldsymbol{X}} := \boldsymbol{H}_0^1 = \left\{\boldsymbol{v}\in[H^1(\Omega)]^d : \boldsymbol{v}=\boldsymbol{0} \text{ on } \partial\Omega\right\},$$

with $\boldsymbol{H}^{-1}$ its dual space, and the pressure space: $Q := H^1(\Omega) \cap L^2_0(\Omega)$, being:

$$L^2_0(\Omega) = \left\{ q \in L^2(\Omega) : \int_\Omega q \, d\boldsymbol{x} = 0 \right\}.$$

We denote by $(\cdot,\cdot)$ the $L^2(\Omega)$-inner product, either for scalar or vector functions. We also denote by $\|\cdot\|_0$ the norm defined by this inner product, and $\langle\cdot,\cdot\rangle$ the duality pairing between $\boldsymbol{H}^{-1}$ and $\boldsymbol{H}^1_0$. Finally, we denote by:

$$\boldsymbol{X} := \boldsymbol{H}_0(div,\Omega) = \{\boldsymbol{v} \in \boldsymbol{L}^2 : \nabla\cdot\boldsymbol{v} \in L^2(\Omega), \boldsymbol{v}\cdot\boldsymbol{n} = 0 \text{ on } \partial\Omega\},$$

the corrected velocity space. Therefore, the variational formulation of the time-splitting scheme previously described reads:

Step 1. Prediction-diffusion problem.
Given $\boldsymbol{f}^{n+1} \in \boldsymbol{H}^{-1}$, $\boldsymbol{u}^n \in \boldsymbol{X}$, and $p^n \in Q$, find $\tilde{\boldsymbol{u}}^{n+1} \in \tilde{\boldsymbol{X}}$ such that:

$$\frac{1}{\Delta t}(\tilde{\boldsymbol{u}}^{n+1} - \boldsymbol{u}^n, \tilde{\boldsymbol{v}}) + \nu(\nabla\tilde{\boldsymbol{u}}^{n+1}, \nabla\tilde{\boldsymbol{v}}) - (p^n, \nabla\cdot\tilde{\boldsymbol{u}}^{n+1}) = \langle \boldsymbol{f}^{n+1}, \tilde{\boldsymbol{v}}\rangle \quad \forall\tilde{\boldsymbol{v}} \in \tilde{\boldsymbol{X}}. \quad (7)$$

Step 2. Pressure-correction problem.
Find $\phi^{n+1} \in Q$ such that:

$$(\nabla\phi^{n+1}, \nabla q) = -\frac{1}{\Delta t}(\nabla\cdot\tilde{\boldsymbol{u}}^{n+1}, q) \quad \forall q \in Q. \quad (8)$$

Step 3. Updating velocity and pressure problem.
Find $\boldsymbol{u}^{n+1} \in \boldsymbol{X}$ and $p^{n+1} \in Q$ such that:

$$(\boldsymbol{u}^{n+1}, \boldsymbol{v}) = (\tilde{\boldsymbol{u}}^{n+1}, \boldsymbol{v}) - \Delta t(\nabla\phi^{n+1}, \boldsymbol{v}) \quad \forall\boldsymbol{v} \in \boldsymbol{X}, \quad (9)$$

$$(p^{n+1}, q) = (p^n, q) + (\phi^{n+1}, q) \quad \forall q \in Q. \quad (10)$$

2.2 FE space approximation

In this section, we define the Finite Element (FE) discretization of the Goda time-splitting method previously described.

In order to give a FE approximation of (7)-(10), let $\{\mathcal{T}_h\}_{h>0}$ be a family of affine-equivalent, conforming and regular triangulations of $\overline{\Omega}$, formed by triangles or quadrilaterals ($d = 2$), tetrahedra or hexahedra ($d = 3$). For any mesh cell $K \in \mathcal{T}_h$, the diameter will be denoted by h_K and $h = \max_{K\in\mathcal{T}_h} h_K$. We consider $\tilde{\boldsymbol{X}}_h \subset \tilde{\boldsymbol{X}}$, $\boldsymbol{X}_h \subset \boldsymbol{X}$ and $Q_h \subset Q$ being suitable FE for the unknown fields. Let us also consider the discrete space of divergence-free functions:

$$\boldsymbol{V}_h = \{\boldsymbol{v}_h \in \boldsymbol{X}_h : (\nabla\cdot\boldsymbol{v}_h, q_h) \quad \forall q_h \in Q_h\}.$$

The FE approximation of (7)-(10) can be written step by step as follows:
Step 1. Prediction-diffusion FE approximation.

Given $\boldsymbol{f}^{n+1} \in \boldsymbol{H}^{-1}$, $\boldsymbol{u}_h^n \in \boldsymbol{X}_h$, *and* $p_h^n \in Q_h$, *find* $\tilde{\boldsymbol{u}}_h^{n+1} \in \tilde{\boldsymbol{X}}_h$ *such that:*

$$\frac{1}{\Delta t}(\tilde{\boldsymbol{u}}_h^{n+1} - \boldsymbol{u}_h^n, \tilde{\boldsymbol{v}}_h) + \nu(\nabla\tilde{\boldsymbol{u}}_h^{n+1}, \nabla\tilde{\boldsymbol{v}}_h) - (p_h^n, \nabla\cdot\tilde{\boldsymbol{u}}_h) = \langle \boldsymbol{f}, \tilde{\boldsymbol{v}}_h\rangle \quad \forall\tilde{\boldsymbol{v}}_h \in \tilde{\boldsymbol{X}}_h, \quad (11)$$

where the initial velocity condition $\boldsymbol{u}_h^0$ is taken as a stable approximation to $\boldsymbol{u}_0$ in L^2-norm belonging to $\boldsymbol{X}_h$ (similarly for pressure). **Step 2.** Pressure-correction FE approximation.

Find $\phi_h^{n+1} \in Q_h$ *such that:*

$$(\nabla\phi_h^{n+1}, \nabla q_h) = -\frac{1}{\Delta t}(\nabla\cdot\tilde{\boldsymbol{u}}_h^{n+1}, q_h) \quad \forall q_h \in Q_h. \quad (12)$$

Step 3. Updating velocity and pressure FE approximation.

Find $\boldsymbol{u}_h^{n+1} \in \boldsymbol{X}_h$ *and* $p_h^{n+1} \in Q_h$ *such that:*

$$\begin{aligned} (\boldsymbol{u}_h^{n+1}, \boldsymbol{v}_h) &= (\tilde{\boldsymbol{u}}_h^{n+1}, \boldsymbol{v}_h) - \Delta t(\nabla\phi_h^{n+1}, \boldsymbol{v}_h) \quad \forall\boldsymbol{v}_h \in \boldsymbol{X}_h, & (13)\\ (p_h^{n+1}, q_h) &= (p_h^n, q_h) + (\phi_h^{n+1}, q_h) \quad \forall q_h \in Q_h. & (14)\end{aligned}$$

3 Goda time-splitting POD-ROM

In this section, we describe the reduced order modeling for the fully discrete time-splitting FOM (11)-(14).

First of all, we briefly recall the Proper Orthogonal Decomposition (POD) method [31] that we will use to construct the Reduced Order Model (ROM). The POD method essentially provides a low dimensional orthonormal basis for representing a given set of data in a certain least-squares optimal sense. The most common version of the POD method is the so-called method of "snapshots".

The key requirement for a computationally efficient ROM is the offline/online (completely separated) decomposition. In the offline phase, one performs the high-costly computation of FOM aimed at building the involved POD bases and corresponding matrices. In the online phase, one solves the ROM for the desired parameter of interest at very low computational cost. Hereafter, we describe these phases applied to the fully discrete FOM (11)-(14).

3.1 POD-ROM

Let us consider the ensembles of unknown snapshots, given by the FOM solutions to (11)-(14) at time t_n, with $n = 1, \ldots, N$:

- $\boldsymbol{S}_{\tilde{u}} = \text{span}\{\tilde{\boldsymbol{u}}_h^1, \ldots, \tilde{\boldsymbol{u}}_h^N\}$ (Predicted velocity snapshots),

- $\boldsymbol{S}_u = \text{span}\{\boldsymbol{u}_h^1, \ldots, \boldsymbol{u}_h^N\}$ (Corrected velocity snapshots),
- $S_p = \text{span}\{p_h^1, \ldots, p_h^N\}$ (Pressure snapshots).

The POD method seeks low-dimensional bases $\{\tilde{\boldsymbol{\varphi}}_1, \ldots, \tilde{\boldsymbol{\varphi}}_{r_{\tilde{u}}}\}$, $\{\boldsymbol{\varphi}_1, \ldots, \boldsymbol{\varphi}_{r_u}\}$, and $\{\psi_1, \ldots, \psi_{r_p}\}$ in real Hilbert spaces $\mathcal{H}_{\tilde{u}}$, $\mathcal{H}_u$, and $\mathcal{H}_p$, respectively, which optimally approximate the snapshots with respect to the corresponding norms [31]. It can be shown that the following POD projection error formulas hold [24, 31]:

$$\Delta t \sum_{n=1}^{N} \left\| \tilde{\boldsymbol{u}}_h^n - \sum_{i=1}^{r_{\tilde{u}}} (\tilde{\boldsymbol{u}}_h^n, \tilde{\boldsymbol{\varphi}}_i)_{\mathcal{H}_{\tilde{u}}} \tilde{\boldsymbol{\varphi}}_i \right\|_{\mathcal{H}_{\tilde{u}}}^2 = \sum_{i=r_{\tilde{u}}+1}^{M_{\tilde{u}}} \tilde{\lambda}_i, \tag{15}$$

$$\Delta t \sum_{n=1}^{N} \left\| \boldsymbol{u}_h^n - \sum_{i=1}^{r_u} (\boldsymbol{u}_h^n, \boldsymbol{\varphi}_i)_{\mathcal{H}_u} \boldsymbol{\varphi}_i \right\|_{\mathcal{H}_u}^2 = \sum_{i=r_u+1}^{M_u} \lambda_i, \tag{16}$$

$$\Delta t \sum_{n=1}^{N} \left\| p_h^n - \sum_{i=1}^{r_p} (p_h^n, \psi_i)_{\mathcal{H}_p} \psi_i \right\|_{\mathcal{H}_p}^2 = \sum_{i=r_p+1}^{M_p} \gamma_i, \tag{17}$$

where $M_{\tilde{u}}$, M_u, and M_p are the rank of $S_{\tilde{u}}$, S_u, and S_p, respectively, and $\tilde{\lambda}_i$, λ_i, and γ_i are the associated eigenvalues. Although $\mathcal{H}_{\tilde{u}}$, $\mathcal{H}_u$, and $\mathcal{H}_p$ can be any real Hilbert spaces, in what follows we consider $\mathcal{H}_{\tilde{u}} = \mathcal{H}_u = \boldsymbol{L}^2$, and $\mathcal{H}_p = H^1$. Note that, in this last case, we consider $(\cdot, \cdot)_{H^1} = (\nabla \cdot, \nabla \cdot)$, and $\| \cdot \|_{H^1} = \| \nabla \cdot \|_0$. With this choice, as we will see in next section, the computation of the reduced corrected velocity and pressure will not need any resolution of linear system, but will directly follow by explicit formulas for the corresponding time coefficients.

We respectively consider the following unknown spaces for the POD setting:

- $\tilde{\boldsymbol{X}}_r = \text{ span}\{\tilde{\boldsymbol{\varphi}}_1, \ldots, \tilde{\boldsymbol{\varphi}}_{r_{\tilde{u}}}\} \subset \tilde{\boldsymbol{X}}_h$ (Predicted velocity POD space),
- $\boldsymbol{X}_r = \text{ span}\{\boldsymbol{\varphi}_1, \ldots, \boldsymbol{\varphi}_{r_u}\} \subset \boldsymbol{X}_h$ (Corrected velocity POD space),
- $Q_r = \text{ span}\{\psi_1, \ldots, \psi_{r_p}\} \subset Q_h$ (Pressure POD space).

Remark 3.1. *Since the POD modes are linear combinations of the snapshots, thus the POD predicted velocity modes satisfy homogeneous Dirichlet boundary conditions, while the POD corrected velocity modes are solenoidal. Thus, the POD corrected velocity modes belong to $\boldsymbol{V}_h$, which yields $\boldsymbol{X}_r \subset \boldsymbol{V}_h$.*

The standard Galerkin projection-based POD-ROM uses both Galerkin truncation and Galerkin projection. The former yields an approximation of the unknown fields by a linear combination of the corresponding truncated POD basis:

$$\tilde{\boldsymbol{u}}(\boldsymbol{x}, t) \approx \tilde{\boldsymbol{u}}_r(\boldsymbol{x}, t) = \sum_{i=1}^{r_{\tilde{\boldsymbol{u}}}} \tilde{a}_i(t) \tilde{\boldsymbol{\varphi}}_i(\boldsymbol{x}) \in \tilde{\boldsymbol{X}}_r, \tag{18}$$

$$\boldsymbol{u}(\boldsymbol{x},t) \approx \boldsymbol{u}_r(\boldsymbol{x},t) = \sum_{i=1}^{r_{\boldsymbol{u}}} a_i(t)\boldsymbol{\varphi}_i(\boldsymbol{x}) \in \boldsymbol{X}_r, \tag{19}$$

$$p(\boldsymbol{x},t) \approx p_r(\boldsymbol{x},t) = \sum_{i=1}^{r_p} b_i(t)\psi_i(\boldsymbol{x}) \in Q_r, \tag{20}$$

where $\{\tilde{a}_i(t)\}_{i=1}^{r_{\tilde{u}}}$, $\{a_i(t)\}_{i=1}^{r_u}$, and $\{b_i(t)\}_{i=1}^{r_p}$ are the sought time-varying coefficients representing the POD-Galerkin trajectories for each field, respectively. Note that the dimension of these unknown vectors is much smaller than the number of degrees of freedom in a full order simulation.

Replacing the FE solution $(\tilde{\boldsymbol{u}}_h^{n+1}, \boldsymbol{u}_h^{n+1}, p_h^{n+1})$ with $(\tilde{\boldsymbol{u}}_r^{n+1}, \boldsymbol{u}_r^{n+1}, p_r^{n+1})$ in (11)-(14) and projecting the resulted equations onto the respective POD spaces using the corresponding POD bases $\{\tilde{\boldsymbol{\varphi}}_i\}_{i=1}^{r_{\tilde{\boldsymbol{u}}}}$, $\{\boldsymbol{\varphi}_i\}_{i=1}^{r_{\boldsymbol{u}}}$, $\{\psi_i\}_{i=1}^{r_p}$, respectively, the full space-time discretization of the proposed POD-ROM reads as:

- **Initialization.** Set:

$$\boldsymbol{u}_r^0 = \sum_{i=1}^{r_{\boldsymbol{u}}} (\boldsymbol{u}_h^0, \boldsymbol{\varphi}_i)\boldsymbol{\varphi}_i, \quad p_r^0 = \sum_{i=1}^{r_p} (\nabla p_h^0, \nabla\psi_i)\psi_i. \tag{21}$$

- **Iteration.** For $n = 0, \ldots, N-1$:

Step 1. Prediction-diffusion reduced order problem.

Given $\boldsymbol{f}^{n+1} \in \boldsymbol{H}^{-1}$, $\boldsymbol{u}_r^n \in \boldsymbol{X}_r$, and $p_r^n \in Q_r$, find $\tilde{\boldsymbol{u}}_r^{n+1} \in \tilde{\boldsymbol{X}}_r$ such that:

$$\left(\frac{\tilde{\boldsymbol{u}}_r^{n+1} - \boldsymbol{u}_r^n}{\Delta t}, \tilde{\boldsymbol{\varphi}}\right) + \nu(\nabla\tilde{\boldsymbol{u}}_r^{n+1}, \nabla\tilde{\boldsymbol{\varphi}}) - (p_r^n, \nabla\cdot\tilde{\boldsymbol{\varphi}}) = \langle \boldsymbol{f}^{n+1}, \tilde{\boldsymbol{\varphi}}\rangle \quad \forall\tilde{\boldsymbol{\varphi}} \in \tilde{\boldsymbol{X}}_r. \tag{22}$$

Step 2. Updating velocity and pressure reduced order problem.

Find $\boldsymbol{u}_r^{n+1} \in \boldsymbol{X}_r$ and $p_r^{n+1} \in \mathcal{Q}_r$ such that:

$$(\boldsymbol{u}_r^{n+1}, \boldsymbol{\varphi}) = (\tilde{\boldsymbol{u}}_r^{n+1}, \boldsymbol{\varphi}) \quad \forall\boldsymbol{\varphi} \in \boldsymbol{X}_r, \tag{23}$$

$$(\nabla p_r^{n+1}, \nabla\psi) = (\nabla p_r^n, \nabla\psi) - \frac{1}{\Delta t}(\nabla\cdot\tilde{\boldsymbol{u}}_r^{n+1}, \psi) \quad \forall\psi \in Q_r, \tag{24}$$

where in (23) we have used that $\boldsymbol{X}_r \subset \boldsymbol{V}_h$, as pointed out in Remark 3.1.

The POD-ROM (22)-(24) yields the following reduced algebraic problems for the unknown vectors of time coefficients:

- **Initialization.** Set:

$$a_i^0 = (\boldsymbol{u}_h^0, \boldsymbol{\varphi}_i) \qquad \text{for } i = 1, \ldots, r_u,$$

$$b_i^0 = (\nabla p_h^0, \nabla\psi_i) \qquad \text{for } i = 1, \ldots, r_p.$$

- **Iteration.** For $n = 0, \ldots, N-1$:

Step 1. Prediction-diffusion algebraic reduced order problem.

Given the vectors of corrected velocity and pressure time coefficients $\boldsymbol{a}^n$, $\boldsymbol{b}^n$, *respectively, compute the vector of predicted velocity time coefficients* $\tilde{\boldsymbol{a}}^{n+1}$ *by:*

$$\left(\frac{1}{\Delta t}\tilde{\boldsymbol{M}} + \nu\tilde{\boldsymbol{S}}\right)\tilde{\boldsymbol{a}}^{n+1} = \frac{1}{\Delta t}\tilde{\boldsymbol{M}}\boldsymbol{a}^n + \boldsymbol{D}\boldsymbol{b}^n + \boldsymbol{c}^{n+1}, \tag{25}$$

where the terms in (25) are evaluated by:

$$\begin{aligned}
\tilde{M}_{ji} &= (\tilde{\boldsymbol{\varphi}}_i, \tilde{\boldsymbol{\varphi}}_j) \qquad \text{for } i,j = 1,\ldots,r_{\tilde{u}},\\
\tilde{S}_{ji} &= (\nabla\tilde{\boldsymbol{\varphi}}_i, \nabla\tilde{\boldsymbol{\varphi}}_j) \quad \text{for } i,j = 1,\ldots,r_{\tilde{u}},\\
D_{ji} &= (\psi_i, \nabla\cdot\tilde{\boldsymbol{\varphi}}_j) \quad \text{for } i = 1,\ldots,r_p \text{ and } j = 1,\ldots,r_{\tilde{u}},\\
c_j &= \langle \boldsymbol{f}^{n+1}, \tilde{\boldsymbol{\varphi}}_j\rangle \quad \text{for } j = 1,\ldots,r_{\tilde{u}}.
\end{aligned} \tag{26}$$

and are precomputed during the offline stage. In (25), $\tilde{\boldsymbol{M}}$ and $\tilde{\boldsymbol{S}}$ are, respectively, the POD mass and stiffness matrices, $\boldsymbol{D}$ is the matrix associated to the pressure term, and $\boldsymbol{c}$ is vector associated to the forcing term. Since we chose to construct the POD predicted velocity basis in $\boldsymbol{L}^2$, then the mass matrix $\tilde{\boldsymbol{M}}$ coincides with the identity matrix.

Step 2. Updating velocity and pressure algebraic reduced order problem.

Compute the vector of corrected velocity and pressure time coefficient $\boldsymbol{a}^{n+1}$, $\boldsymbol{b}^{n+1}$, *respectively, by:*

$$\boldsymbol{a}^{n+1} = \hat{\boldsymbol{M}}\tilde{\boldsymbol{a}}^{n+1}, \tag{27}$$

$$\boldsymbol{b}^{n+1} = \boldsymbol{b}^n - \frac{1}{\Delta t}\boldsymbol{D}^T\tilde{\boldsymbol{a}}^{n+1}, \tag{28}$$

where $\hat{\boldsymbol{M}}$ in (27) is defined element-wise as:

$$\hat{M}_{ji} = (\tilde{\boldsymbol{\varphi}}_i, \boldsymbol{\varphi}_j) \text{ for } i = 1,\ldots,r_{\tilde{\boldsymbol{u}}} \text{ and } j = 1,\ldots,r_{\boldsymbol{u}}, \tag{29}$$

and $\boldsymbol{D}$ in (28) has been defined in (26). Again, the involved matrices are precomputed during the offline stage.

4 Analysis of the time-splitting Goda-ROM

In this section, we perform the numerical analysis of the proposed Goda time-splitting POD-ROM (22)-(24), dealing with stability and error estimates.

4.1 Technical background

This section provides some technical results that are required for the numerical analysis. Throughout the paper, we shall denote by C a positive constant that may vary from one line to another but that is always independent of the viscosity ν, the FE mesh size h, the time step Δt, and the corrected velocity, predicted velocity and pressure eigenvalues $\lambda_i, \tilde{\lambda}_i, \gamma_i$, respectively.

Definition 4.1. *Let X be a Hilbert space and Y, Z two finite-dimensional subspaces of X with intersection reduced to the zero function. The pair of finite-dimensional spaces (Y, Z) is called to satisfy the saturation property if there exists a positive constant C such that:*

$$\|y\|_X + \|z\|_X \leq C\|y + z\|_X \quad \forall y \in Y, z \in Z. \tag{30}$$

The saturation property can be viewed as an inverse triangular inequality.

Lemma 4.2. *(see [40], Lemma 5.3). The saturation property is equivalent to the existence of a constant $\alpha < 1$ such that:*

$$|(y, z)_X| \leq \alpha\|y\|_X\|z\|_X \quad \forall y \in Y, z \in Z. \tag{31}$$

We may take $\alpha = 1 - 2/C^2$ (see Remark 2 in [5]), and in the sequel we will call α the saturation constant. Then, we can interpret the saturation property in the sense that the angle between spaces Y and Z, defined by:

$$\theta = \arccos\left(\sup_{y\in Y\setminus\{0\}, z\in Z\setminus\{0\}} \frac{(y, z)_X}{\|y\|_X\|z\|_X}\right), \tag{32}$$

is uniformly bounded from below by a positive angle, and $\alpha = \cos(\theta)$.

Remark 4.3. *Lemma 4.2 will be used in Theorem 4.8 to bound the error term arising from Step 2 of the pressure estimate.*

Note that the argument of saturation property has been used in [5] to develop a stabilized post-processing of the Galerkin FE solution of convection-dominated flows and was very recently extended [2] to POD-ROM approximations to propose a cure for instabilities due to advection-dominance in POD solution to advection-diffusion-reaction equations [38].

It also gave a mathematical argument to perform the numerical analysis of recently proposed stabilization POD-ROMs [9, 40] that take into account the pressure instability for incompressible flows governed by the Navier–Stokes equations.

4.2 Existence and stability results for Goda-ROM

We have the following existence and stability result for the proposed Goda-ROM, (22)-(24):

Theorem 4.4 (Existence and stability results for Goda-ROM)**.** *The Goda-ROM* (22)-(24) *admits a unique solution that satisfies the following bounds:*

$$\max_{0\leq k\leq N}\|\boldsymbol{u}_r^k\|_0^2 \leq \|\tilde{\boldsymbol{u}}_r^0\|_0^2 + \Delta t^2\|\nabla p_r^0\|_0^2 + \nu^{-1}\sum_{n=0}^{N-1}\Delta t\|\boldsymbol{f}^{n+1}\|_{\boldsymbol{H}^{-1}}^2. \tag{33}$$

$$\begin{aligned}&\max_{0\leq k\leq N}\|\tilde{\boldsymbol{u}}_r^k\|_0^2 + \nu\sum_{n=0}^{N-1}\Delta t\|\nabla\tilde{\boldsymbol{u}}_r^{n+1}\|_0^2 + \Delta t^2\max_{0\leq k\leq N}\|\nabla p_r^k\|_0^2\\ \leq\ &\|\tilde{\boldsymbol{u}}_r^0\|_0^2 + \Delta t^2\|\nabla p_r^0\|_0^2 + \nu^{-1}\sum_{n=0}^{N-1}\Delta t\|\boldsymbol{f}^{n+1}\|_{\boldsymbol{H}^{-1}}^2.\end{aligned} \tag{34}$$

Proof. Problem (22)-(24) is equivalent to a square linear system of $(r_{\tilde{u}} + r_u + r_p)$ equations at each time step. Therefore, uniqueness of the solution is equivalent to its existence. Let us assume that there exists a solution and prove that it is unique. Actually, this will follow from (33)-(34), thus we will prove these estimates.

- **Corrected velocity stability estimate.**

Taking $\boldsymbol{\varphi} = \boldsymbol{u}_r^{n+1}$ in (23), and applying Cauchy–Schwarz and Young's inequalities we obtain:

$$\|\boldsymbol{u}_r^{n+1}\|_0^2 \leq \|\tilde{\boldsymbol{u}}_r^{n+1}\|_0^2. \tag{35}$$

Hence, from (35) we have:

$$\max_{0\leq k\leq N}\|\boldsymbol{u}_r^k\|_0^2 \leq \max_{0\leq k\leq N}\|\tilde{\boldsymbol{u}}_r^k\|_0^2. \tag{36}$$

Estimate (33) follows from (36) by proving (34) in next step.

- **Predicted velocity-pressure stability estimate.**

By projecting equation (13) onto the predicted reduced velocity POD space $\tilde{\boldsymbol{X}}_r$ for the reduced velocity at time n and integrating by parts we obtain:

$$(\boldsymbol{u}_r^n, \tilde{\boldsymbol{\varphi}}) = (\tilde{\boldsymbol{u}}_r^n, \tilde{\boldsymbol{\varphi}}) + \Delta t(p_r^n - p_r^{n-1}, \nabla\cdot\tilde{\boldsymbol{\varphi}}) \quad \forall\tilde{\boldsymbol{\varphi}} \in \tilde{\boldsymbol{X}}_r. \tag{37}$$

Substituting (37) into (22) we get:

$$\left(\frac{\tilde{\boldsymbol{u}}_r^{n+1}-\tilde{\boldsymbol{u}}_r^n}{\Delta t},\tilde{\boldsymbol{\varphi}}\right)+\nu(\nabla\tilde{\boldsymbol{u}}_r^{n+1},\nabla\tilde{\boldsymbol{\varphi}})-(2p_r^n-p_r^{n-1},\nabla\cdot\tilde{\boldsymbol{\varphi}})=\langle\boldsymbol{f}^{n+1},\tilde{\boldsymbol{\varphi}}\rangle, \tag{38}$$

for all $\tilde{\boldsymbol{\varphi}}\in\tilde{\boldsymbol{X}}_r$.

To prove estimate (34), we set $\tilde{\boldsymbol{\varphi}}=2\Delta t\tilde{\boldsymbol{u}}_r^{n+1}$ in (38), $\psi=2\Delta t^2(2p_r^n-p_r^{n-1})$ in (24), and add both equations. Using the polarization identity:

$$\left(\frac{\tilde{\boldsymbol{u}}_r^{n+1}-\tilde{\boldsymbol{u}}_r^n}{\Delta t},2\Delta t\tilde{\boldsymbol{u}}_r^{n+1}\right)=\|\tilde{\boldsymbol{u}}_r^{n+1}\|_0^2-\|\tilde{\boldsymbol{u}}_r^n\|_0^2+\|\tilde{\boldsymbol{u}}_r^{n+1}-\tilde{\boldsymbol{u}}_r^n\|_0^2,$$

we obtain:

$$\begin{aligned}&\|\tilde{\boldsymbol{u}}_r^{n+1}\|_0^2+\|\tilde{\boldsymbol{u}}_r^{n+1}-\tilde{\boldsymbol{u}}_r^n\|_0^2+2\Delta t\nu\|\nabla\tilde{\boldsymbol{u}}_r^{n+1}\|_0^2\\ +\;&2\Delta t^2(\nabla(p_r^{n+1}-p_r^n),\nabla(2p_r^n-p_r^{n-1}))=\|\tilde{\boldsymbol{u}}_r^n\|_0^2+2\Delta t\langle f^{n+1},\tilde{\boldsymbol{u}}_r^{n+1}\rangle.\end{aligned} \tag{39}$$

From (24) at time t^n, we have:

$$\Delta t(\nabla(p_r^n-p_r^{n-1}),\nabla\psi)+(\nabla\cdot\tilde{\boldsymbol{u}}_r^n,\psi)=0. \tag{40}$$

Subtracting (40) from (24) and taking $\psi=2\Delta t(p_r^{n+1}-p_r^n)$, we get:

$$-2\Delta t(\tilde{\boldsymbol{u}}_r^{n+1}-\tilde{\boldsymbol{u}}_r^n,\nabla(p_r^{n+1}-p_r^n))+2\Delta t^2(\nabla(p_r^{n+1}-2p_r^n+p_r^{n-1}),\nabla(p_r^{n+1}-p_r^n))=0. \tag{41}$$

Summing (39) and (41), we have:

$$\begin{aligned}&\|\tilde{\boldsymbol{u}}_r^{n+1}\|_0^2+\|\tilde{\boldsymbol{u}}_r^{n+1}-\tilde{\boldsymbol{u}}_r^n\|_0^2+2\Delta t\nu\|\nabla\tilde{\boldsymbol{u}}_r^{n+1}\|_0^2\\ &+\Delta t^2(\|\nabla p_r^{n+1}\|_0^2+\|\nabla(p_r^{n+1}-p_r^n)\|_0^2)\\ =\;&\|\tilde{\boldsymbol{u}}_r^n\|_0^2+\Delta t^2\|\nabla p_r^n\|_0^2+2\Delta t\langle f^{n+1},\tilde{\boldsymbol{u}}_r^{n+1}\rangle+2\Delta t(\tilde{\boldsymbol{u}}_r^{n+1}-\tilde{\boldsymbol{u}}_r^n,\nabla(p_r^{n+1}-p_r^n))\\ \leq\;&\|\tilde{\boldsymbol{u}}_r^n\|_0^2+\Delta t^2\|\nabla p_r^n\|_0^2+\Delta t\left(\frac{\|\boldsymbol{f}^{n+1}\|_{\boldsymbol{H}^{-1}}}{\nu}+\nu\|\nabla\tilde{\boldsymbol{u}}_r^{n+1}\|_0^2\right)\\ &+\Delta t\left(\|\tilde{\boldsymbol{u}}_r^{n+1}-\tilde{\boldsymbol{u}}_r^n\|_0^2+\|\nabla(p_r^{n+1}-p_r^n)\|_0^2\right).\end{aligned} \tag{42}$$

where in the last inequality we have used the definition of the dual norm and Young's inequality. From (42), we get:

$$\begin{aligned}&\|\tilde{\boldsymbol{u}}_r^{n+1}\|_0^2+\Delta t\nu\|\nabla\tilde{\boldsymbol{u}}_r^{n+1}\|_0^2+\Delta t^2\|\nabla p_r^{n+1}\|_0^2\\ \leq\;&\|\tilde{\boldsymbol{u}}_r^n\|_0^2+\Delta t^2\|\nabla p_n^r\|_0^2+\frac{\Delta t}{\nu}\|\boldsymbol{f}^{n+1}\|_{\boldsymbol{H}^{-1}}^2.\end{aligned} \tag{43}$$

By summing (43) from $n=0$ to $k<N$, we get (34).

□

Remark 4.5. *Note that the presence of the factor Δt^2 in front of the pressure term is inherent to the time-splitting scheme, and it can also be found in stability and convergence results of full order time-splitting scheme for incompressible flows, see e.g. [20].*

4.2.1 Alternative pressure stability estimate for Goda-ROM

An alternative pressure stability estimate for the Goda-ROM (22)-(24), following Corollary 5.13 in [40], could be obtained. To do so, let us define the norm:

$$|||\cdot||| = \sup_{\tilde{\boldsymbol{\varphi}}\in\tilde{\boldsymbol{X}}_{\boldsymbol{r}}} \frac{(\cdot, \nabla\cdot\tilde{\boldsymbol{\varphi}})}{\|\nabla\tilde{\boldsymbol{\varphi}}\|_0} + \sqrt{\Delta t}\|\nabla\cdot\|_0. \tag{44}$$

The following result holds:

Corollary 4.6. *The time primitive of the reduced pressure satisfies the following stability bound:*

$$\sqrt{\Delta t}\max_{1\le n\le N}|||2\mathcal{P}_r^n - \mathcal{P}_r^{n-1}||| \le C\left[\|\tilde{\boldsymbol{u}}_r^0\|_0 + \Delta t\|\nabla p_r^0\|_0 + \frac{1}{\sqrt{\nu}}\left(\sum_{k=0}^{N-1}\Delta t\|\boldsymbol{f}^{k+1}\|^2_{\boldsymbol{H}^{-1}}\right)^{\frac{1}{2}}\right], \tag{45}$$

where $\mathcal{P}_r^n = \sum_{k=0}^{n}\Delta t p_r^k$.

Proof. For any $\tilde{\boldsymbol{\varphi}} \in \tilde{\boldsymbol{X}}_r$, from (38) we get:

$$(2p_r^n - p_r^{n-1}, \nabla\cdot\tilde{\boldsymbol{\varphi}}) = \left(\frac{\tilde{\boldsymbol{u}}_r^{n+1} - \tilde{\boldsymbol{u}}_r^n}{\Delta t}, \tilde{\boldsymbol{\varphi}}\right) + \nu(\nabla\tilde{\boldsymbol{u}}_r^{n+1}, \nabla\tilde{\boldsymbol{\varphi}}) - \langle \boldsymbol{f}^{n+1}, \tilde{\boldsymbol{\varphi}}\rangle.$$

Then, summation over the discrete times gives:

$$(2\mathcal{P}_r^n - \mathcal{P}_r^{n-1}, \nabla\cdot\tilde{\boldsymbol{\varphi}}) = (\tilde{\boldsymbol{u}}_r^{n+1} - \tilde{\boldsymbol{u}}_r^0, \tilde{\boldsymbol{\varphi}}) + \sum_{k=0}^{n}\Delta t[\nu(\nabla\tilde{\boldsymbol{u}}_r^{k+1}, \nabla\tilde{\boldsymbol{\varphi}}) - \langle \boldsymbol{f}^{n+1}, \tilde{\boldsymbol{\varphi}}\rangle]. \tag{46}$$

Thus, from (46) we get:

$$\begin{aligned} &\sup_{\tilde{\boldsymbol{\varphi}}\in\tilde{\boldsymbol{X}}_r} \frac{(2\mathcal{P}_r^n - \mathcal{P}_r^{n-1}, \nabla\cdot\tilde{\boldsymbol{\varphi}})}{\|\nabla\tilde{\boldsymbol{\varphi}}\|_0} + \sqrt{\Delta t}\|\nabla(2\mathcal{P}_r^n - \mathcal{P}_r^{n-1})\|_0 \\ \le\ & \|\tilde{\boldsymbol{u}}_r^{n+1}\|_0 + \|\tilde{\boldsymbol{u}}_r^0\|_0 + \sum_{k=0}^{n}\Delta t(\nu\|\nabla\tilde{\boldsymbol{u}}_r^{k+1}\|_0 + \|\boldsymbol{f}^{k+1}\|_{\boldsymbol{H}^{-1}}) \\ &+\sqrt{\Delta t}\|\nabla(2\mathcal{P}_r^n - \mathcal{P}_r^{n-1})\|_0, \end{aligned} \tag{47}$$

where we have applied the triangle inequality, the Cauchy–Schwarz inequality, and the definition of the dual norm. So, if we use the norm definition (44), by the

Cauchy–Schwarz inequality, from (47) we have:

$$
\begin{aligned}
|||2\mathcal{P}_r^n - \mathcal{P}_r^{n-1}||| \;\leq\; C \Bigg[& \max_{0\leq k\leq N} \|\tilde{\boldsymbol{u}}_r^k\|_0 + \left(\nu \sum_{k=0}^{N-1} \Delta t \|\nabla \tilde{\boldsymbol{u}}_r^{k+1}\|_0^2 \right)^{\frac{1}{2}} \\
& + \left(\sum_{k=0}^{N-1} \Delta t \|\boldsymbol{f}^{k+1}\|_{\boldsymbol{H}^{-1}}^2 \right)^{\frac{1}{2}} \\
& + \left(\sum_{k=1}^{N} \Delta t^2 \|\nabla(2p_r^n - p_r^{n-1})\|_0^2 \right)^{\frac{1}{2}} \Bigg] . \qquad (48)
\end{aligned}
$$

Using the stability estimate (34) to bound the terms on the right-hand side of (48), we get estimate (45) for the time primitive of the reduced order pressure.

□

Remark 4.7. *Note that the technical trick of considering the time primitive of the reduced order pressure $\mathcal{P}_r$, as originally introduced in [6] for a FE-FOM, allowed to reduce the order of the penalty factor Δt in front of the pressure term.*

4.3 Error estimates for Goda-ROM

We are now in position to state the following POD truncation error estimate between the Goda-ROM solution obtained by (22)-(24) and the snapshot data obtained by the FOM (11)-(14).

Theorem 4.8 (POD truncation error)**.** *Let $(\boldsymbol{u}_h, \tilde{\boldsymbol{u}}_h, p_h)$ be the FOM solution defined in* (11)-(14) *and $(\boldsymbol{u}_r, \tilde{\boldsymbol{u}}_r, p_r)$ be the Goda-ROM solution defined in* (22)-(24)*. Then, the following bounds hold:*

$$
\begin{aligned}
\sum_{n=0}^{N-1} \Delta t \|\boldsymbol{u}_h^{n+1} - \boldsymbol{u}_r^{n+1}\|_0^2 \;\leq\; & C\, T\, e^T \left(\sum_{i=r_{\tilde{u}}+1}^{M_{\tilde{u}}} \tilde{\lambda}_i \left(\Delta t^{-2} + \|\nabla \tilde{\boldsymbol{\varphi}}_i\|_0^2 \right) + \nu^{-1} \sum_{i=r_p+1}^{M_p} \gamma_i \|\psi_i\|_0^2 \right) \\
& + \sum_{i=r_u+1}^{M_u} \lambda_i . \qquad (49)
\end{aligned}
$$

$$\sum_{n=0}^{N-1}\Delta t\|\tilde{\boldsymbol{u}}_h^{n+1}-\tilde{\boldsymbol{u}}_r^{n+1}\|_0^2+\nu\sum_{n=0}^{N-1}\Delta t\|\nabla(\tilde{\boldsymbol{u}}_h^{n+1}-\tilde{\boldsymbol{u}}_r^{n+1})\|_0^2$$
$$+\Delta t^2\sum_{n=0}^{N-1}\Delta t\|\nabla(p_h^{n+1}-p_r^{n+1})\|_0^2$$
$$\leq \; C\,T\,e^T\left(\sum_{i=r_{\tilde{u}}+1}^{M_{\tilde{u}}}\tilde{\lambda}_i\left(\Delta t^{-2}+\|\nabla\tilde{\boldsymbol{\varphi}}_i\|_0^2\right)+\nu^{-1}\sum_{i=r_p+1}^{M_p}\gamma_i\|\psi_i\|_0^2\right). \qquad (50)$$

Proof. Let us denote by:

$$\boldsymbol{\eta}_h^n=P_r^u\boldsymbol{u}_h^n-\boldsymbol{u}_h^n,\qquad \tilde{\boldsymbol{\eta}}_h^n=P_r^{\tilde{u}}\tilde{\boldsymbol{u}}_h^n-\tilde{\boldsymbol{u}}_h^n,\qquad \zeta_h^n=P_r^p p_h^n-p_h^n,$$

where P_r^u and $P_r^{\tilde{u}}$ denote the L^2-orthogonal projection on $\boldsymbol{X}_r$ and $\tilde{\boldsymbol{X}}_r$, respectively, and P_r^p is the elliptic projection on Q_r. For these projections, we have the following POD projection error estimates that we will use in the sequel:

- *L^2-POD projection error estimates.*

$$\begin{aligned}\Delta t\sum_{n=1}^{N}\|\boldsymbol{\eta}_h^n\|_0^2 &= \sum_{i=r_u+1}^{M_u}\lambda_i,\quad \Delta t\sum_{n=1}^{N}\|\tilde{\boldsymbol{\eta}}_h^n\|_0^2=\sum_{i=r_{\tilde{u}}+1}^{M_{\tilde{u}}}\tilde{\lambda}_i,\\ \Delta t\sum_{n=1}^{N}\|\zeta_h^n\|_0^2 &= \sum_{i=r_p+1}^{M_p}\gamma_i\|\psi_i\|_0^2. \end{aligned}\qquad (51)$$

- *H^1-POD projection error estimates.*

$$\begin{aligned}\Delta t\sum_{n=1}^{N}\|\nabla\boldsymbol{\eta}_h^n\|_0^2 &= \sum_{i=r_u+1}^{M_u}\lambda_i\|\nabla\boldsymbol{\varphi}_i\|_0^2,\quad \Delta t\sum_{n=1}^{N}\|\nabla\tilde{\boldsymbol{\eta}}_h^n\|_0^2=\sum_{i=r_{\tilde{u}}+1}^{M_{\tilde{u}}}\tilde{\lambda}_i\|\nabla\tilde{\boldsymbol{\varphi}}_i\|_0^2,\\ \Delta t\sum_{n=1}^{N}\|\nabla\zeta_h^n\|_0^2 &= \sum_{i=r_p+1}^{M_p}\gamma_i. \end{aligned}\qquad (52)$$

Note that the first two estimates in (51) and last estimate in (52) directly follow from (15)-(17), while for the rest we refer to [30], Lemma 2.2.

- **Corrected velocity error estimate.**

For the projection of the corrected velocity, from (13) we get:

$$(P_r^u\boldsymbol{u}_h^{n+1},\boldsymbol{\varphi})=(P_r^u\tilde{\boldsymbol{u}}_h^{n+1},\boldsymbol{\varphi})\quad\forall\boldsymbol{\varphi}\in\boldsymbol{X}_r. \qquad (53)$$

Let us denote by:

$$\boldsymbol{e}_r^n = \boldsymbol{u}_r^n - P_r^u \boldsymbol{u}_h^n.$$

Subtracting (53) from the ROM equation (23) we get:

$$(\boldsymbol{e}_r^{n+1}, \boldsymbol{\varphi}) = (\tilde{\boldsymbol{u}}_r^{n+1} - P_r^u \tilde{\boldsymbol{u}}_h^{n+1}, \boldsymbol{\varphi}) = (\tilde{\boldsymbol{u}}_r^{n+1} - P_r^u \tilde{\boldsymbol{u}}_h^{n+1} \pm \tilde{\boldsymbol{u}}_h^{n+1}, \boldsymbol{\varphi}). \tag{54}$$

Taking $\boldsymbol{\varphi} = \boldsymbol{e}_r^{n+1}$, from (54) we obtain:

$$\|\boldsymbol{e}_r^{n+1}\|_0^2 \leq \|\tilde{\boldsymbol{u}}_h^{n+1} - \tilde{\boldsymbol{u}}_r^{n+1}\|_0^2. \tag{55}$$

Multiplying by Δt, summing from $n = 0$ to $k < N$, using the triangle inequality and the first POD projection error estimate in (51), from (55) we derive:

$$\sum_{n=0}^{N-1} \Delta t \|\boldsymbol{u}_h^{n+1} - \boldsymbol{u}_r^{n+1}\|_0^2 \leq \sum_{n=0}^{N-1} \Delta t \|\tilde{\boldsymbol{u}}_h^{n+1} - \tilde{\boldsymbol{u}}_r^{n+1}\|_0^2 + \sum_{i=r_u+1}^{M_u} \lambda_i. \tag{56}$$

Estimate (49) follows from (56) by proving (50) in next step.

- **Predicted velocity-pressure error estimate.**

By testing equation (13) on $\tilde{\boldsymbol{X}}_h$ at time n and integrating by parts we obtain:

$$(\boldsymbol{u}_h^n, \tilde{\boldsymbol{v}}_h) = (\tilde{\boldsymbol{u}}_h^n, \tilde{\boldsymbol{v}}_h) + \Delta t (p_h^n - p_h^{n-1}, \nabla \cdot \tilde{\boldsymbol{v}}_h) \quad \forall \tilde{\boldsymbol{v}}_h \in \tilde{\boldsymbol{X}}_h. \tag{57}$$

Substituting (57) into (11), we get:

$$\left(\frac{\tilde{\boldsymbol{u}}_h^{n+1} - \tilde{\boldsymbol{u}}_h^n}{\Delta t}, \tilde{\boldsymbol{v}}_h \right) + \nu (\nabla \tilde{\boldsymbol{u}}_h^{n+1}, \nabla \tilde{\boldsymbol{v}}_h) - (2p_h^n - p_h^{n-1}, \nabla \cdot \tilde{\boldsymbol{v}}_h) = \langle \boldsymbol{f}^{n+1}, \tilde{\boldsymbol{v}}_h \rangle, \tag{58}$$

for all $\tilde{\boldsymbol{v}}_h \in \tilde{\boldsymbol{X}}_h$.

For the projection of the predicted velocity, for all $\tilde{\boldsymbol{\varphi}} \in \tilde{\boldsymbol{X}}_r$ from (58) we get:

$$\begin{aligned} & \left(\frac{P_r^{\tilde{u}}(\tilde{\boldsymbol{u}}_h^{n+1} - \tilde{\boldsymbol{u}}_h^n)}{\Delta t}, \tilde{\boldsymbol{\varphi}} \right) + \nu (\nabla P_r^{\tilde{u}} \tilde{\boldsymbol{u}}_h^{n+1}, \nabla \tilde{\boldsymbol{\varphi}}) \\ = \; & \langle \boldsymbol{f}^{n+1}, \tilde{\boldsymbol{\varphi}} \rangle + (P_r^p (2p_h^n - p_h^{n-1}), \nabla \cdot \tilde{\boldsymbol{\varphi}}) + \nu (\nabla \tilde{\boldsymbol{\eta}}_h^{n+1}, \nabla \tilde{\boldsymbol{\varphi}}) \\ & - (2\zeta_h^n - \zeta_h^{n-1}, \nabla \cdot \tilde{\boldsymbol{\varphi}}). \end{aligned} \tag{59}$$

For the projection of the pressure correction, for all $\psi \in \mathcal{Q}_r$ from (12) we get:

$$\left(\nabla P_r^p (p_h^{n+1} - p_h^n), \nabla \psi \right) = -\frac{1}{\Delta t} (\nabla \cdot P_r^{\tilde{u}} \tilde{\boldsymbol{u}}_h^{n+1}, \psi) + \frac{1}{\Delta t} (\nabla \cdot \tilde{\boldsymbol{\eta}}_h^{n+1}, \psi). \tag{60}$$

Let us denote by:

$$\tilde{\boldsymbol{e}}_r^n = \tilde{\boldsymbol{u}}_r^n - P_r^{\tilde{u}} \tilde{\boldsymbol{u}}_h^n, \qquad z_r^n = p_r^n - P_r^p p_h^n.$$

Subtracting (59) from (38) we get:

$$\begin{aligned}&\left(\frac{\tilde{\boldsymbol{e}}_r^{n+1}-\tilde{\boldsymbol{e}}_r^{n}}{\Delta t},\tilde{\boldsymbol{\varphi}}\right)+\nu(\nabla\tilde{\boldsymbol{e}}_r^{n+1},\nabla\tilde{\boldsymbol{\varphi}})\\ =\;&(2z_r^n-z_r^{n-1},\nabla\cdot\tilde{\boldsymbol{\varphi}})-\nu(\nabla\tilde{\boldsymbol{\eta}}_h^{n+1},\nabla\tilde{\boldsymbol{\varphi}})+(2\zeta_h^n-\zeta_h^{n-1},\nabla\cdot\tilde{\boldsymbol{\varphi}}),\end{aligned}\tag{61}$$

for all $\tilde{\boldsymbol{\varphi}}\in\tilde{\boldsymbol{X}}_r$, and subtracting (60) from (24) we get:

$$\big(\nabla(z_r^{n+1}-z_r^n),\nabla\psi\big)=-\frac{1}{\Delta t}(\nabla\cdot\tilde{\boldsymbol{e}}_r^{n+1},\psi)-\frac{1}{\Delta t}(\nabla\cdot\tilde{\boldsymbol{\eta}}_h^{n+1},\psi),\tag{62}$$

for all $\psi\in\mathcal{Q}_r$.

Taking $\tilde{\boldsymbol{\varphi}}=\tilde{\boldsymbol{e}}_r^{n+1}$ in (61) and integrating by parts we obtain:

$$\begin{aligned}&\frac{1}{2\Delta t}\left(\|\tilde{\boldsymbol{e}}_r^{n+1}\|_0^2+\|\tilde{\boldsymbol{e}}_r^{n+1}-\tilde{\boldsymbol{e}}_r^{n}\|_0^2-\|\tilde{\boldsymbol{e}}_r^{n}\|_0^2\right)+\nu\|\nabla\tilde{\boldsymbol{e}}_r^{n+1}\|_0^2+\nu(\nabla\tilde{\boldsymbol{\eta}}_h^{n+1},\nabla\tilde{\boldsymbol{e}}_r^{n+1})\\&+\big(\nabla(2z_r^n-z_r^{n-1}),\tilde{\boldsymbol{e}}_r^{n+1}\big)+\big(\nabla(2\zeta_h^n-\zeta_h^{n-1}),\tilde{\boldsymbol{e}}_r^{n+1}\big)=0.\end{aligned}\tag{63}$$

and taking $\psi=2\,z_r^n-z_r^{n-1}$ in (62) and integrating by parts we obtain:

$$\begin{aligned}&-\big(\tilde{\boldsymbol{e}}_r^{n+1},\nabla(2z_r^n-z_r^{n-1})\big)-\big(\tilde{\boldsymbol{\eta}}_h^{n+1},\nabla(2z_r^n-z_r^{n-1})\big)\\&+\Delta t\,\big(\nabla(z_r^{n+1}-z_r^n),\nabla(2z_r^n-z_r^{n-1})\big)=0.\end{aligned}\tag{64}$$

From (62) at time t^n, we have:

$$\Delta t\,\big(\nabla(z_r^n-z_r^{n-1}),\nabla\psi\big)+(\nabla\cdot\tilde{\boldsymbol{e}}_r^n,\psi)+(\nabla\cdot\tilde{\boldsymbol{\eta}}_h^n,\psi)=0,\tag{65}$$

for all $\psi\in\mathcal{Q}_r$.

Subtracting (65) from (62) and taking $\psi=z_r^{n+1}-z_r^n$ we get:

$$\begin{aligned}&-\big(\tilde{\boldsymbol{e}}_r^{n+1}-\tilde{\boldsymbol{e}}_r^{n},\nabla(z_r^{n+1}-z_r^n)\big)-\big(\tilde{\boldsymbol{\eta}}_h^{n+1}-\tilde{\boldsymbol{\eta}}_h^{n},\nabla(z_r^{n+1}-z_r^n)\big)\\&+\Delta t\,\big(\nabla(z_r^{n+1}-2z_r^n+z_r^{n-1}),\nabla(z_r^{n+1}-z_r^n)\big)=0.\end{aligned}\tag{66}$$

Summing (63), (64) and (66) we have:

$$\begin{aligned}&\frac{1}{2\Delta t}\left(\|\tilde{\boldsymbol{e}}_r^{n+1}\|_0^2+\|\tilde{\boldsymbol{e}}_r^{n+1}-\tilde{\boldsymbol{e}}_r^{n}\|_0^2-\|\tilde{\boldsymbol{e}}_r^{n}\|_0^2\right)+\nu\|\nabla\tilde{\boldsymbol{e}}_r^{n+1}\|_0^2\\&+\frac{1}{2}\Delta t\left(\|\nabla z_r^{n+1}\|_0^2+\|\nabla(z_r^{n+1}-z_r^n)\|_0^2-\|\nabla z_r^n\|_0^2\right)\\=\;&-\nu(\nabla\tilde{\boldsymbol{\eta}}_h^{n+1},\nabla\tilde{\boldsymbol{e}}_r^{n+1})-\big(\nabla(2\zeta_h^n-\zeta_h^{n-1}),\tilde{\boldsymbol{e}}_r^{n+1}\big)+\big(\tilde{\boldsymbol{\eta}}_h^{n+1},\nabla(2z_r^n-z_r^{n-1})\big)\\&+\big(\tilde{\boldsymbol{e}}_r^{n+1}-\tilde{\boldsymbol{e}}_r^{n},\nabla(z_r^{n+1}-z_r^n)\big)+\big(\tilde{\boldsymbol{\eta}}_h^{n+1}-\tilde{\boldsymbol{\eta}}_h^{n},\nabla(z_r^{n+1}-z_r^n)\big)=\sum_{i=1}^{5}A_i.\end{aligned}\tag{67}$$

We will bound the $\{A_i\}_{i=1}^5$ terms on the right-hand side of (67). For the first three terms we get:

$$A_1 \leq \frac{\varepsilon_1^{-1}\nu}{4}\|\nabla\tilde{\boldsymbol{\eta}}_h^{n+1}\|_0^2 + \varepsilon_1\nu\|\nabla\tilde{\boldsymbol{e}}_r^{n+1}\|_0^2, \tag{68}$$

$$A_2 \leq \frac{\varepsilon_2^{-1}}{4}\|2\zeta_h^n - \zeta_h^{n-1}\|_0^2 + \varepsilon_2\|\nabla\tilde{\boldsymbol{e}}_r^{n+1}\|_0^2, \tag{69}$$

$$A_3 \leq \frac{2}{\Delta t^2}\|\tilde{\boldsymbol{\eta}}_h^{n+1}\|_0^2 + \frac{(\Delta t)^2}{4}\left(\|\nabla z_r^n\|_0^2 + \|\nabla(z_r^n - z_r^{n-1})\|_0^2\right), \tag{70}$$

for some small positive constants ε_1, ε_2 (to be determined later).

For the fourth term, applying Lemma 4.2 with $Y = \tilde{\boldsymbol{X}}_r$ and $Z = \text{span}\{\nabla\psi_1, \ldots, \nabla\psi_{r_p}\}$ we have:

$$A_4 \leq \alpha\frac{\Delta t}{2}\left\|\frac{\tilde{\boldsymbol{e}}_r^{n+1} - \tilde{\boldsymbol{e}}_r^n}{\Delta t}\right\|_0^2 + \alpha\frac{\Delta t}{2}\|\nabla(z_r^{n+1} - z_r^n)\|_0^2. \tag{71}$$

Finally, for the fifth term:

$$A_5 \leq \frac{1}{2}\left\|\frac{\tilde{\boldsymbol{\eta}}_h^{n+1} - \tilde{\boldsymbol{\eta}}_h^n}{\Delta t}\right\|_0^2 + \frac{\Delta t^2}{2}\|\nabla(z_r^{n+1} - z_r^n)\|_0^2. \tag{72}$$

Inserting inequalities (68)-(72) into (67), multiplying by $2\,\Delta t$ and taking $\varepsilon_1 = 1/4$, $\varepsilon_2 = \nu/4$, we obtain:

$$\begin{aligned}
&\|\tilde{\boldsymbol{e}}_r^{n+1}\|_0^2 - \|\tilde{\boldsymbol{e}}_r^n\|_0^2 + (1-\alpha)\Delta t^2\left\|\frac{\tilde{\boldsymbol{e}}_r^{n+1} - \tilde{\boldsymbol{e}}_r^n}{\Delta t}\right\|_0^2 + \nu\Delta t\|\nabla\tilde{\boldsymbol{e}}_r^{n+1}\|_0^2 \\
&+\Delta t^2\left(\|\nabla z_r^{n+1}\|_0^2 - \|\nabla z_r^n\|_0^2 + (1-(\Delta t+\alpha))\|\nabla(z_r^{n+1} - z_r^n)\|_0^2\right) \\
\leq\ & \frac{1}{2}\Delta t^3\|\nabla z_r^n\|_0^2 + \frac{1}{2}\Delta t^3\|\nabla(z_r^n - z_r^{n-1})\|_0^2 + 2\nu\Delta t\|\nabla\tilde{\boldsymbol{\eta}}_h^{n+1}\|_0^2 \\
&+\frac{2}{\nu}\Delta t\|2\zeta_h^n - \zeta_h^{n-1}\|_0^2 + \frac{4}{\Delta t}\|\tilde{\boldsymbol{\eta}}_h^{n+1}\|_0^2 + \Delta t\left\|\frac{\tilde{\boldsymbol{\eta}}_h^{n+1} - \tilde{\boldsymbol{\eta}}_h^n}{\Delta t}\right\|_0^2.
\end{aligned} \tag{73}$$

Summing (73) from $n=0$ to $k<N$ and assuming $\Delta t < \frac{2}{3}(1-\alpha)$ we have:

$$\begin{aligned}
&\|\tilde{\boldsymbol{e}}_r^{k+1}\|_0^2 + \nu \sum_{n=0}^{k} \Delta t \|\nabla \tilde{\boldsymbol{e}}_r^{n+1}\|_0^2 + \Delta t^2 \|\nabla z_r^{k+1}\|_0^2 \\
\leq\ & \|\tilde{\boldsymbol{e}}_r^{0}\|_0^2 + \Delta t^2 \|\nabla z_r^{0}\|_0^2 + \frac{1}{2}\Delta t \sum_{n=0}^{k} \Delta t^2 \|\nabla z_r^{n}\|_0^2 + 2\nu \sum_{n=0}^{k} \Delta t \|\nabla \tilde{\boldsymbol{\eta}}_h^{n+1}\|_0^2 \\
&+ \frac{2}{\nu} \sum_{n=0}^{k} \Delta t \|2\zeta_h^{n+1} - \zeta_h^n\|_0^2 + \frac{4}{\Delta t^2} \sum_{n=0}^{k} \Delta t \|\tilde{\boldsymbol{\eta}}_h^{n+1}\|_0^2 + \sum_{n=0}^{k} \Delta t \left\| \frac{\tilde{\boldsymbol{\eta}}_h^{n+1} - \tilde{\boldsymbol{\eta}}_h^{n}}{\Delta t} \right\|_0^2 \\
=\ & \|\tilde{\boldsymbol{e}}_r^{0}\|_0^2 + \Delta t^2 \|\nabla z_r^{0}\|_0^2 + \frac{1}{2}\Delta t \sum_{n=0}^{k} \Delta t^2 \|\nabla z_r^{n}\|_0^2 + \sum_{i=1}^{4} B_i^k. \qquad (74)
\end{aligned}$$

Applying Gronwall's lemma (see for instance [23], Lemma 5.1) we get:

$$\begin{aligned}
&\max_{0\leq k\leq N} \|\tilde{\boldsymbol{e}}_r^{k}\|_0^2 + \nu \sum_{n=0}^{N-1} \Delta t \|\nabla \tilde{\boldsymbol{e}}_r^{n+1}\|_0^2 + \max_{0\leq k\leq N} \Delta t^2 \|\nabla z_r^{k}\|_0^2 \\
\leq\ & e^T \left(\|\tilde{\boldsymbol{e}}_r^{0}\|_0^2 + \Delta t^2 \|\nabla z_r^{0}\|_0^2 + 2 \sum_{i=1}^{4} B_i^{N-1} \right). \qquad (75)
\end{aligned}$$

By using POD projection error estimates (51)-(52), we can bound the $\{B_i^{N-1}\}_{i=1}^4$ terms on the right-hand side of (75) obtaining:

$$\begin{aligned}
&\max_{0\leq k\leq N} \|\tilde{\boldsymbol{e}}_r^{k}\|_0^2 + \nu \sum_{n=0}^{N-1} \Delta t \|\nabla \tilde{\boldsymbol{e}}_r^{n+1}\|_0^2 + \max_{0\leq k\leq N} \Delta t^2 \|\nabla z_r^{k}\|_0^2 \\
\leq\ & e^T \left(\|\tilde{\boldsymbol{e}}_r^{0}\|_0^2 + \Delta t^2 \|\nabla z_r^{0}\|_0^2 + C \sum_{i=r_{\tilde{u}}+1}^{M_{\tilde{u}}} \tilde{\lambda}_i \left(\Delta t^{-2} + \|\nabla \tilde{\boldsymbol{\varphi}}_i\|_0^2 \right) \right) \\
&+ \frac{e^T C}{\nu} \sum_{i=r_p+1}^{M_p} \gamma_i \|\psi_i\|_0^2. \qquad (76)
\end{aligned}$$

Taking the ROM initial conditions as the POD projection of the FOM initial solutions, as indicated in (21), then (76) reads:

$$\begin{aligned}
&\max_{1\leq k\leq N} \|\tilde{\boldsymbol{e}}_r^{k}\|_0^2 + \nu \sum_{n=0}^{N-1} \Delta t \|\nabla \tilde{\boldsymbol{e}}_r^{n+1}\|_0^2 + \max_{1\leq k\leq N} \Delta t^2 \|\nabla z_r^{k}\|_0^2 \\
\leq\ & e^T C \left(\sum_{i=r_{\tilde{u}}+1}^{M_{\tilde{u}}} \tilde{\lambda}_i \left(\Delta t^{-2} + \|\nabla \tilde{\boldsymbol{\varphi}}_i\|_0^2 \right) + \nu^{-1} \sum_{i=r_p+1}^{M_p} \gamma_i \|\psi_i\|_0^2 \right). \qquad (77)
\end{aligned}$$

Finally, using the inequality:

$$\sum_{n=0}^{N-1} \Delta t \|\tilde{\boldsymbol{e}}_r^{n+1}\|_0^2 \leq T \max_{1\leq k\leq N} \|\tilde{\boldsymbol{e}}_r^k\|_0^2,$$

$$\sum_{n=0}^{N-1} \Delta t \|\nabla z_r^{n+1}\|_0^2 \leq T \max_{1\leq k\leq N} \|\nabla z_r^k\|_0^2,$$

the triangle inequality and the POD projection error estimates (51)-(52), we reach error bound (50).

□

Remark 4.9. *Let us observe that all the terms in the error bounds* (49)-(50) *are written in terms of the discarded eigenvalues, since we have directly compared the Goda-ROM solution to the snapshot data, by using their projections onto the corresponding ROM spaces as in [34], instead of projections of the continuous solution (see, for example, [26, 28, 7, 40]).*

On the other hand, note that the error bounds (49)-(50) *depend on* ν^{-1}*. This problem could be overtaken considering an additional grad-div stabilization term in the prediction-diffusion step in order to obtain error bounds independent of inverse powers of the viscosity, as done for instance in [14, 15, 34] in the ROM framework.*

Remark 4.10. *If we consider to build the POD basis for both velocities in* H^1*, we get the following error estimates:*

$$\begin{aligned}\sum_{n=0}^{N-1} \Delta t \|\boldsymbol{u}_h^{n+1} - \boldsymbol{u}_r^{n+1}\|_0^2 \;\leq\; & C\,T\,e^T \left(\sum_{i=r_{\tilde{u}}+1}^{M_{\tilde{u}}} \tilde{\lambda}_i \Delta t^{-2} + \nu^{-1} \sum_{i=r_p+1}^{M_p} \gamma_i \|\psi_i\|_0^2 \right) \\ & + \sum_{i=r_u+1}^{M_u} \lambda_i. \end{aligned} \tag{78}$$

$$\begin{aligned} & \sum_{n=0}^{N-1} \Delta t \|\tilde{\boldsymbol{u}}_h^{n+1} - \tilde{\boldsymbol{u}}_r^{n+1}\|_0^2 + \nu \sum_{n=0}^{N-1} \Delta t \|\nabla(\tilde{\boldsymbol{u}}_h^{n+1} - \tilde{\boldsymbol{u}}_r^{n+1})\|_0^2 \\ & + \Delta t^2 \sum_{n=0}^{N-1} \Delta t \|\nabla(p_h^{n+1} - p_r^{n+1})\|_0^2 \\ \leq\; & C\,T\,e^T \left(\sum_{i=r_{\tilde{u}}+1}^{M_{\tilde{u}}} \tilde{\lambda}_i (\nu^{-1}+1) \Delta t^{-2} + \nu^{-1} \sum_{i=r_p+1}^{M_p} \gamma_i \|\psi_i\|_0^2 \right). \end{aligned} \tag{79}$$

The proof of (78)-(79) *follows along the same lines of Theorem 4.8, except for the* A_1 *term in* (68) *that now reads:*

$$A_1 = -\left(\frac{\tilde{\boldsymbol{\eta}}_h^{n+1} - \tilde{\boldsymbol{\eta}}_h^n}{\Delta t}, \tilde{\boldsymbol{e}}_r^{n+1}\right) \leq \frac{\varepsilon_1^{-1}\nu}{4}\left\|\frac{\tilde{\boldsymbol{\eta}}_h^{n+1} - \tilde{\boldsymbol{\eta}}_h^n}{\Delta t}\right\|_0^2 + C_p^2\varepsilon_1\|\nabla\tilde{\boldsymbol{e}}_r^{n+1}\|_0^2, \tag{80}$$

where we have applied Cauchy–Schwarz, Young and Poincaré (with constant C_p*) inequalities.*

Remark 4.11. *Let us observe that if we just limit the error analysis to the computation of error estimates between the ROM solution and the projection of the snapshot data onto the corresponding ROM spaces, then* ℓ^∞ *in time errors can be obtained for both velocities and pressure, see estimate* (77)*. However, when considering the error between the ROM solution and the snapshot data, then the error in time is limited to* ℓ^2*, unless Difference Quotients (DQs) [31, 25] in the snapshots ensambles are used to maintain* ℓ^∞ *in time errors (see e.g. [10, 11, 12, 13, 27, 29, 30] for recent works with DQs in the ROM context).*

The use of DQs could also be benefit to improve error estimates (78)-(79) *when one considers the POD basis for both velocities in* H^1*, since in that case the coefficient* $(\nu^{-1}+1)\Delta t^{-2}$ *would be replaced by* $(\nu^{-1}+\Delta t^{-2})$*.*

4.3.1 Alternative pressure error estimate for Goda-ROM

An alternative pressure error estimate for the Goda-ROM (22)-(24), following Corollary 5.18 in [40], could be obtained in the norm defined in (44), which could be weaker than the L^2-norm in the ROM context, see Remark 4.8 in [34].

The following result holds:

Corollary 4.12. *The time primitive of the reduced pressure satisfies the following error estimate:*

$$\sqrt{\Delta t}\max_{1\leq n\leq N}|||(2\mathcal{P}_h^n - \mathcal{P}_h^{n-1}) - (2\mathcal{P}_r^n - \mathcal{P}_r^{n-1})||| \leq C\sqrt{E}, \tag{81}$$

where E *denotes the right-hand side of the inequality* (77)*, and* $\mathcal{P}_h^n = \displaystyle\sum_{k=0}^{n}\Delta t p_h^k$*,* $\mathcal{P}_r^n = \displaystyle\sum_{k=0}^{n}\Delta t p_r^k$*.*

Proof. For any $\tilde{\boldsymbol{\varphi}} \in \tilde{\boldsymbol{X}}_r$, from (61) we get:

$$(2z_r^n - z_r^{n-1}, \nabla\cdot\tilde{\boldsymbol{\varphi}}) = \left(\frac{\tilde{\boldsymbol{e}}_r^{n+1} - \tilde{\boldsymbol{e}}_r^n}{\Delta t}, \tilde{\boldsymbol{\varphi}}\right) + \nu(\nabla\tilde{\boldsymbol{e}}_r^{n+1}, \nabla\tilde{\boldsymbol{\varphi}}) + \langle\boldsymbol{\varepsilon}_h^{n+1}, \tilde{\boldsymbol{\varphi}}\rangle,$$

with $\boldsymbol{\varepsilon}_h^{n+1}$ denoting the consistency error, defined as:

$$\langle \boldsymbol{\varepsilon}_h^{n+1}, \tilde{\boldsymbol{\varphi}} \rangle = \nu(\nabla \tilde{\boldsymbol{\eta}}_h^{n+1}, \nabla \tilde{\boldsymbol{\varphi}}) - (2\zeta_h^n - \zeta_h^{n-1}, \nabla \cdot \tilde{\boldsymbol{\varphi}}).$$

Let $Z_r^n = \sum_{k=0}^n \Delta t z_r^k = \sum_{k=0}^n \Delta t (p_r^k - P_r^p p_h^k)$. Then, summation over the discrete times gives:

$$(2Z_n^r - Z_r^{n-1}, \nabla \cdot \tilde{\boldsymbol{\varphi}}) = (\tilde{\boldsymbol{e}}_r^{n+1}, \tilde{\boldsymbol{\varphi}}) + \sum_{k=0}^{n} \Delta t \left[\nu(\nabla \tilde{\boldsymbol{e}}_r^{k+1}, \nabla \tilde{\boldsymbol{\varphi}}) + \langle \boldsymbol{\varepsilon}_h^{k+1}, \tilde{\boldsymbol{\varphi}} \rangle \right], \tag{82}$$

by taking the ROM initial conditions as the POD projection of the FOM initial solutions, as indicated in (21). Thus, from (82) we get:

$$\begin{aligned} & \sup_{\tilde{\boldsymbol{\varphi}} \in \tilde{\boldsymbol{X}}_r} \frac{(2Z_r^n - Z_r^{n-1}, \nabla \cdot \tilde{\boldsymbol{\varphi}})}{\|\nabla \tilde{\boldsymbol{\varphi}}\|} + \sqrt{\Delta t} \|\nabla (2Z_r^n - Z_r^{n-1})\|_0 \\ \leq \; & C \left[\|\tilde{\boldsymbol{e}}_r^{n+1}\|_0 + \sum_{k=0}^{n} \Delta t \left(\nu \|\nabla \tilde{\boldsymbol{e}}_r^{k+1}\|_0 + \|\boldsymbol{\varepsilon}_h^{k+1}\|_{\boldsymbol{H}^{-1}} \right) \right] \\ & + \sqrt{\Delta t} \|\nabla (2Z_r^n - Z_r^{n-1}\|_0, \end{aligned} \tag{83}$$

where we have applied the triangle inequality, the Cauchy–Schwarz inequality, and the definition of the dual norm. So, if we use the norm definition (44), by the Cauchy–Schwarz inequality, from (83) we have:

$$\begin{aligned} |||2Z_r^n - Z_r^{n-1}||| \; \leq \; & C \left[\max_{1 \leq k \leq N} \|\tilde{\boldsymbol{e}}_r^k\|_0 + \left(\nu \sum_{k=0}^{N-1} \Delta t \|\nabla \tilde{\boldsymbol{e}}_r^{k+1}\|_0^2 \right)^{1/2} \right. \\ & + \left(\sum_{k=0}^{N-1} \Delta t \|\boldsymbol{\varepsilon}_h^{k+1}\|_{\boldsymbol{H}^{-1}}^2 \right)^{1/2} \\ & \left. + \left(\sum_{k=1}^{N} \Delta t^2 \|\nabla (2z_r^k - z_r^{k-1})\|_0^2 \right)^{1/2} \right]. \end{aligned} \tag{84}$$

Finally, we obtain:

$$\sqrt{\Delta t} |||2Z_r^n - Z_r^{n-1}||| \leq C\sqrt{E}, \tag{85}$$

where E denotes the right-hand side of the inequality (77). From the triangle inequality and the L^2-POD projection error estimate for pressure (51), we get (81).

□

5 Numerical Studies

In this section, we present numerical results for the Goda-ROM introduced and analyzed in the previous sections. To evaluate the efficiency and effectiveness of the ROM, we conduct three numerical experiments, each with Dirichlet boundary conditions.

In the first experiment, we apply the ROM to a cavity by solving the Stokes equations with a known exact solution, treating time as a parameter. This setup allows us to assess the accuracy of the ROM and evaluate error estimates by directly comparing the proposed model with the exact solution. The second case addresses a scenario involving a singular solution that exhibits a strong coupling between time and space. To achieve this, we adjust the source term data to introduce significant singularity. We will evaluate the approximation error by comparing the ROM solution with the FE solution, providing insights into the ROM's performance in handling highly singular data. Finally, to increase the complexity and test the robustness of the ROM, we solve the Navier–Stokes equations using the lid-driven cavity benchmark problem. Here, we incorporate both time and a physical parameter, the Reynolds number, to observe how the ROM handles variations in fluid dynamics under increased nonlinearity.

All numerical experiments were performed using the open-source FE software FreeFEM [22], which provides a flexible environment for implementing and testing the proposed ROM on these fluid dynamics problems.

These experiments highlight the capabilities of the proposed ROM in various settings, enabling a comprehensive evaluation of its performance under different physical and computational conditions.

5.1 Unsteady Stokes solution

5.1.1 Setup for numerical simulations

For the next two fabricated cases, we consider the computational domain equal to $\Omega = [0,1] \times [0,1] \subset \mathbb{R}^2$, the time interval is $[0,T]$, where $T = 1$, and the viscosity coefficient is $\nu = 1$. The numerical method to get the snapshots is the one described in Section 2.1, with a spatial discretization using $\mathbb{P}^2 - \mathbb{P}^1$ FE for the pair velocity-pressure on a relatively coarse computational grid, for which we consider a uniform partition of the cavity on 64^2 cells, resulting in 33 282 degrees of freedom for velocity and 4 225 degrees of freedom for pressure. In the FOM simulations, the time step considered is $\Delta t = 10^{-2}$. For the ROM, we collect $M = 21$ snapshots for each unknown field, by storing every fourth FOM solution in the time interval $[0.2, 1]$. The POD modes are generated in L^2-norm for velocities and H^1-norm for pressure. In the sequel, we will consider the discrete relative error between the FE

solution s_h and the ROM solution s_r in norm $l^2(L^2)$ given by:

$$\frac{\|s_h - s_r\|_{l^2(L^2)}}{\|s_h\|_{l^2(L^2)}} = \sqrt{\frac{\sum_{i=1}^{M} \|s_h^i - s_r^i\|_0^2}{\sum_{i=1}^{M} \|s_h^i\|_0^2}},$$

for a given field s.

5.1.2 Regular exact solution

The first example concerns a prescribed regular solution given by [32]:

$$\begin{aligned} \boldsymbol{u}(x,y;t) = &\quad \cos(t) \begin{pmatrix} \pi \sin(\pi x)^2 \sin(2\pi y) \\ -\pi \sin(2\pi x) \sin(\pi y)^2 \end{pmatrix}, \\ p(x,y;t) = &\quad 10 \cos(t) \cos(\pi x) \cos(\pi y). \end{aligned} \tag{86}$$

In Figure 1, we show the decay of POD eigenvalues (left) and the captured energy (right) computed by $100 \sum_{k=1}^{r} \lambda_k / \sum_{k=1}^{M} \lambda_k$, where λ_k are the corresponding eigenvalues and M the rank of the corresponding data set of the problem. Note that with 1 POD mode we already capture more than 99% of the energy for each field.

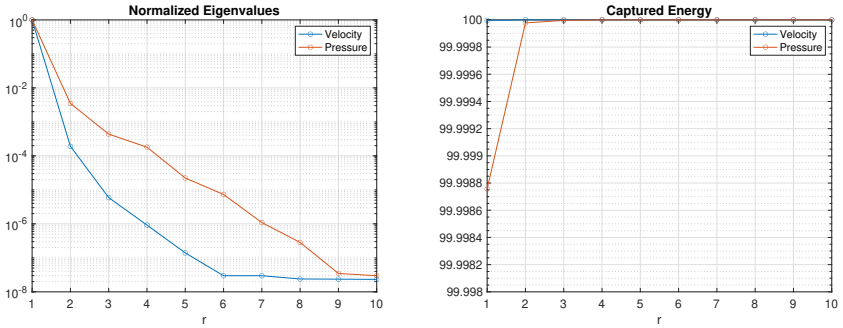

Figure 1: Example 5.1.2: Decay of the normalized POD eigenvalues (left) and captured energy (right).

Figure 2 shows $l^2(L^2)$ relative errors for both velocity (left) and pressure (right). For comparison purposes, we also plot the $l^2(L^2)$ relative projection errors for both velocity and pressure in the same figure. From Figure 2, we observe that with more than 3 velocity modes we get the minimum relative error. However, for pressure, we need more than 5 modes to reach the minimum relative error, which is in agreement with the slower decay of pressure eigenvalues with respect to the velocity ones, see Figure 1.

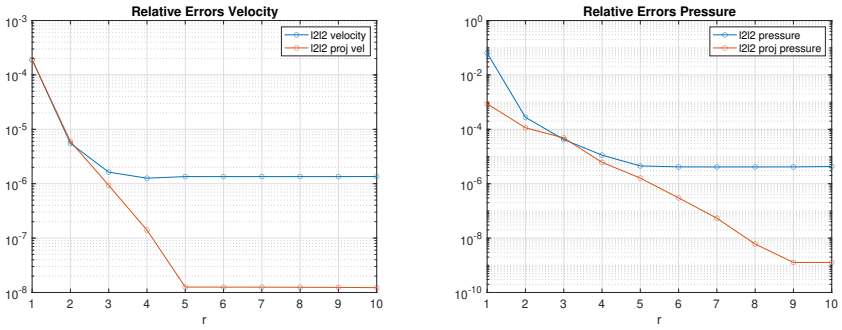

Figure 2: Example 5.1.2: $l^2(L^2)$ relative errors for velocity (left) and pressure (right) with their respective $l^2(L^2)$ projection errors.

5.1.3 Singular model

In the next example, the source term 'suffers' from a strong coupling between time and space. It is defined as

$$\boldsymbol{f}(x, y; t) = \begin{pmatrix} \sqrt{|x + y - 0.3 - t|} \\ \sqrt{|xy - 0.3 - t|} \end{pmatrix}. \tag{87}$$

The corresponding solution to the unsteady Stokes problem is not directly accessible, and it is not expected to exhibit high regularity. We anticipate that it will have a weaker capacity to be represented as a sum of separated functions compared to the previous, more regular case. In particular, the singular values of both the velocity and pressure fields are not expected to decay rapidly, and certainly not exponentially. These singular values, plotted in Fig. 3 on a fully logarithmic scale, appear to exhibit a polynomial decay, and more modes are required to capture 99% of the energy.

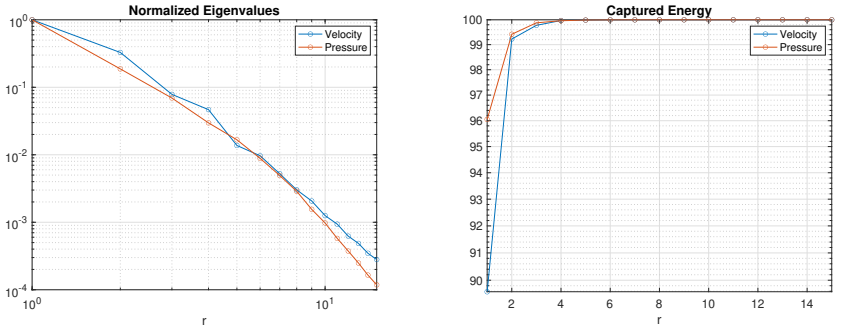

Figure 3: Example 5.1.3: Decay of the normalized POD eigenvalues (left) and captured energy (right).

In Figure 4, we show the comparison between the $l^2(L^2)$ relative error for each field and its respective projection. We note that the $l^2(L^2)$ relative error of each field has the same behaviour of its projection.

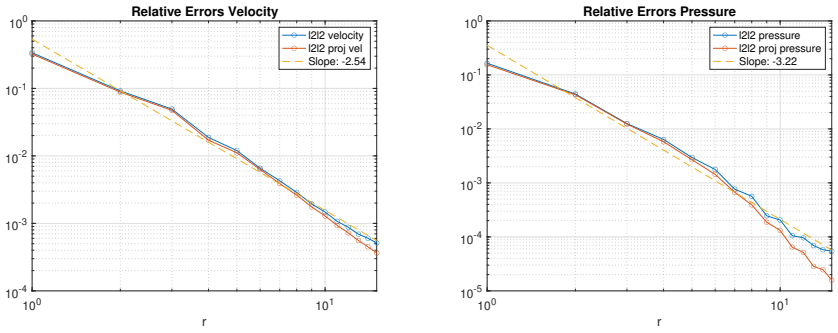

Figure 4: Example 5.1.3: $l^2(L^2)$ relative errors for velocity (left) and pressure (right) with their respective $l^2(L^2)$ projection errors in logarithmic scale for both X and Y axes.

According to polynomial regression, the errors decrease approximately as $r^{-2,54}$ for the velocity and $r^{-3,22}$ for the pressure, which illustrates the singularity of the solution.

5.2 Lid-driven cavity problem

5.2.1 Setup for numerical simulations

The lid-driven cavity problem is one of the most popular validation problems for wall-bounded fluid flow simulations. In this test, the fluid is contained in a unitary squared domain and it has Dirichlet boundary conditions on all sides: three stationary sides and one moving side at the top, characterized by a unitary tangent velocity. The right-hand side of the momentum equation vanishes in Ω, i.e., $\boldsymbol{f} = \mathbf{0}$.

For this test, we also consider the Reynolds number ($Re = 1/\nu$) as a parameter, ranging in $\mathcal{D} = [1\,000, 5\,000]$. In this range of Reynolds number, the solution reaches a steady state regime.

FOM and POD modes. The numerical method to get the snapshots is the one described in Section 2.1, with a spatial discretization using $\mathbb{P}^2 - \mathbb{P}^1$ FE for the pair velocity-pressure on a mesh (see Figure 5) refined towards the walls in both directions to capture the unknown fields with a high precision using the hyperbolic

tangent function [21, 39]:

$$f(x) = 0.5 \left(1 + \frac{\tanh\left(2(2x-1)\right)}{\tanh\left(2\right)} \right). \tag{88}$$

The partition of the cavity is 64^2, resulting in 33 282 degrees of freedom for velocity and 4 225 degrees of freedom for pressure.

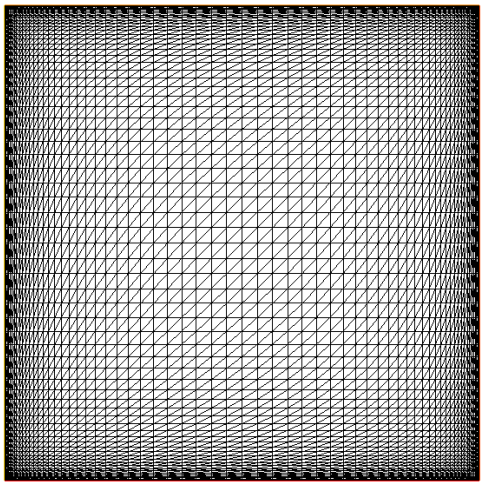

Figure 5: Example 5.2: Computational grid.

In the FOM simulations, an impulsive start is performed, i.e. the initial conditions are zero velocity and pressure fields, and the time step is $\Delta t = 5 \cdot 10^{-3}$. Time integration is performed using the time-splitting method described in Section 2.1. The approach adopted for the treatment of the Navier–Stokes non-linear term $(\boldsymbol{u} \cdot \nabla)\boldsymbol{u}$ involved in the material derivative of the velocity consists in approximating it by $(\boldsymbol{u}^n \cdot \nabla)\tilde{\boldsymbol{u}}^{\boldsymbol{n+1}}$ in the prediction step, thus applying a semi-implicit Euler method.

To compute the ROM, we consider two parameters: the physical parameter Reynolds number Re and the time t, as mentioned earlier. The physical parameter range for the Reynolds number $\mathcal{D} = [1000, 5000]$ is uniformly partitioned into 5 sample points. For the time variable, we capture the solution within the time interval $(2, 3]$, in which the flow has not reached yet a steady-state regime (transitory regime). As a result, we collect $M = 5 \cdot 200 = 1000$ snapshots for each unknown field to construct the ROM. The POD modes are generated using the L^2-norm for velocities and the H^1-norm for pressure. In Figure 6, we illustrate the decay of the normalized eigenvalues (left) and the captured energy, as defined in the previous section. It is noteworthy that with just 5 POD modes, we capture more than 99% of the energy for each field.

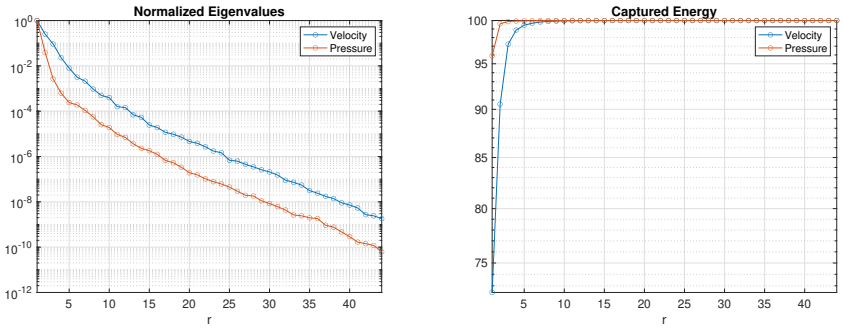

Figure 6: Example 5.2: Decay of the normalized POD eigenvalues (left) and captured energy (right).

5.2.2 Numerical results

With POD modes generated, the ROM is constructed using the same time discretization as for the FOM, and we evaluate the results for different parameter values.

In Figure 7, we show the $l^2(L^2)$ relative error for both velocity and pressure. As for the Stokes problem, we compare these errors with their respective $l^2(L^2)$ relative projection errors, computed for the time instances in which the snapshots were taken.

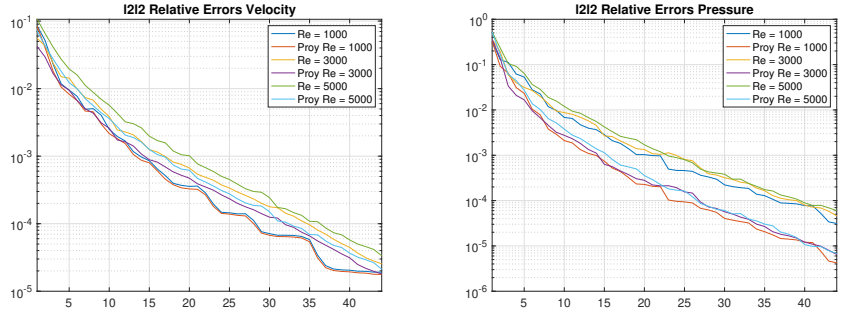

Figure 7: Example 5.2: $l^2(L^2)$ relative errors for velocity (left) and pressure (right) with their respective $l^2(L^2)$ projection errors.

From Figure 7, we observe that the errors have almost the same behaviour as projection errors.

For the time parameter, we also analyze the performance of the ROM with respect to extrapolation. Using three samples of the Reynolds parameter ($Re \in \{1\,000, 3\,000, 5\,000\}$), we evaluate the ROM over the time interval $(2, 4]$, while the snapshots are taken in the time interval $(2, 3]$. To assess the ROM performances

in this context, we plot in Figure 8 the temporal evolution of the L^2 error in space for both velocity (left) and pressure (right).

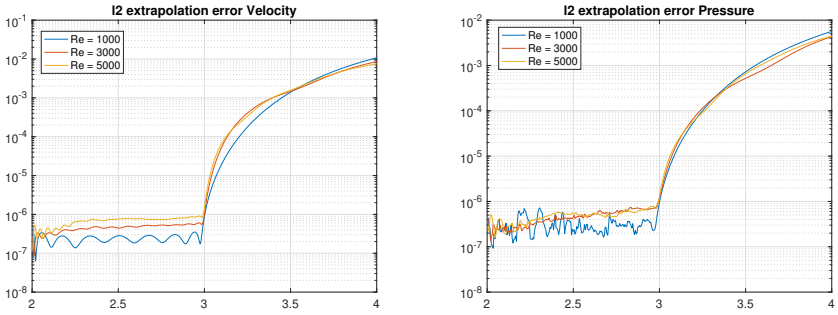

Figure 8: Example 5.2: Temporal evolution of the L^2 error in space for velocity (left) and pressure (right).

From Figure 8, we can observe that the errors are lower than 10^{-6} in the time window in which we compute the snapshots, while they increase up to 10^{-2} in the predictive time interval.

On the other hand, to evaluate the performances of the ROM for different physical parameter Re, we select values of Re inside the range $\mathcal{D} = [1\,000, 5\,000]$, but also different from the chosen samples. In Figure 9, we show the $l^2(L^2)$ relative velocity and pressure errors in the time interval $(2, 3]$ for different values of Reynolds numbers inside $\mathcal{D}$.

From Figure 9, we observe that the velocity error reaches the maximum value of 10^{-2} approximately for $Re = 1\,500$, while for pressure is $5 \cdot 10^{-2}$ approximately.

6 Conclusions

In this paper, we propose a time-splitting POD-ROM, which combines the strength of projection methods with the POD-Galerkin approach. Also, an important point addressed in the current work lies in the choice of the scalar product used to compute the POD modes for each variable in the problem. The proposed approach leads to a fully explicit computation of both pressure and velocity fields. The resulting ROM model is well-posed, and we establish rigorous *a-priori* error estimates for both the pressure and velocity approximations. Numerical experiments are carried out to validate the convergence, efficiency, and stability of the ROM, demonstrating its effectiveness also for the Navier–Stokes equations.

The work presented in this contribution is based on a first-order temporal approximation. Extending this approach to a second-order approximation is straightforward for numerical experiments; however, the theoretical framework demands

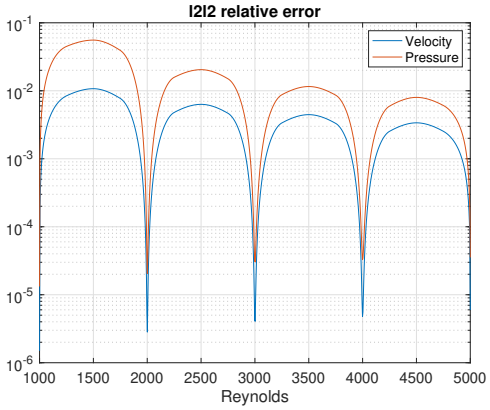

Figure 9: Example 5.2: $l^2(L^2)$ relative velocity and pressure errors in the time interval $(2, 3]$ for different values of Reynolds number inside $\mathcal{D}$.

further refinement. Addressing these technical developments is a priority for future research, where we aim to rigorously establish the numerical analysis for second-order time discretizations. Also, we are extending the present work towards problems with outflow boundary conditions [35, 18] in the ROM context. This study is today in progress.

Acknowledgments: This work has been supported by the Spanish Government Project PID2021-123153OB-C21 and the European Union's Horizon 2020 research and innovation programme under the Marie Sklodowska–Curie Actions, grant agreement 872442 (ARIA). The research of M. Azaïez has been supported by the French National Research Agency ANR-23-ASTR-0003 (SINRAM).

References

[1] M. Azaïez, T. Chacón Rebollo, M. Oulghelou, and I. Sánchez Muñoz. Least-squares pressure recovery in reduced order methods for incompressible flows. *J. Comput. Phys.*, 519:19, 2024. Id/No 113397.

[2] M. Azaïez, T. Chacón Rebollo, and S. Rubino. A cure for instabilities due to advection-dominance in POD solution to advection-diffusion-reaction equations. *J. Comput. Phys.*, 425:27, 2021. Id/No 109916.

[3] F. Ballarin, A. Manzoni, A. Quarteroni, and G. Rozza. Supremizer stabilization of POD-Galerkin approximation of parametrized steady incompressible Navier-Stokes equations. *Int. J. Numer. Methods Eng.*, 102(5):1136–1161, 2015.

[4] K. Carlberg, C. Farhat, J. Cortial, and D. Amsallem. The GNAT method for nonlinear model reduction: effective implementation and application to computational fluid dynamics and turbulent flows. *J. Comput. Phys.*, 242:623–647, 2013.

[5] T. Chacón Rebollo and A. Domínguez Delgado. A unified analysis of mixed and stabilized finite element solutions of Navier-Stokes equations. *Comput. Methods Appl. Mech. Eng.*, 182(3-4):301–331, 2000.

[6] T. Chacón Rebollo and R. Lewandowski. *Mathematical and numerical foundations of turbulence models and applications*. Model. Simul. Sci. Eng. Technol. New York, NY: Birkhäuser/Springer, 2014.

[7] T. Chacón Rebollo, S. Rubino, M. Oulghelou, and C. Allery. Error analysis of a residual-based stabilization-motivated POD-ROM for incompressible flows. *Comput. Methods Appl. Mech. Eng.*, 401:25, 2022. Id/No 115627.

[8] A. J. Chorin. Numerical solution of the Navier-Stokes equations. *Math. Comput.*, 22:745–762, 1968.

[9] V. DeCaria, T. Iliescu, W. Layton, M. McLaughlin, and M. Schneier. An artificial compression reduced order model. *SIAM J. Numer. Anal.*, 58(1):565–589, 2020.

[10] S. L. Eskew and J. R. Singler. A new approach to proper orthogonal decomposition with difference quotients. *Adv. Comput. Math.*, 49(2):33, 2023. Id/No 13.

[11] B. García-Archilla, V. John, S. Katz, and J. Novo. POD-ROMs for incompressible flows including snapshots of the temporal derivative of the full order solution: Error bounds for the pressure. *Journal of Numerical Mathematics*, (0), 2023.

[12] B. García-Archilla, V. John, and J. Novo. POD-ROMs for incompressible flows including snapshots of the temporal derivative of the full order solution. *SIAM J. Numer. Anal.*, 61(3):1340–1368, 2023.

[13] B. García-Archilla, V. John, and J. Novo. Second order error bounds for POD-ROM methods based on first order divided differences. *Appl. Math. Lett.*, 146:7, 2023. Id/No 108836.

[14] B. García-Archilla, J. Novo, and S. Rubino. Error analysis of proper orthogonal decomposition data assimilation schemes with grad-div stabilization for the Navier-Stokes equations. *J. Comput. Appl. Math.*, 411:30, 2022. Id/No 114246.

[15] B. García-Archilla, J. Novo, and S. Rubino. On the influence of the nonlinear term in the numerical approximation of incompressible flows by means of proper orthogonal decomposition methods. *Comput. Methods Appl. Mech. Eng.*, 405:21, 2023. Id/No 115866.

[16] V. Girault and P.-A. Raviart. *Finite Element Approximations of the Navier-Stokes Equations*. New York: Springer, 1986.

[17] K. Goda. A multistep technique with implicit difference schemes for calculating two- or three-dimensional cavity flows. *J. Comput. Phys.*, 30:76–95, 1979.

[18] J. L. Guermond, P. Minev, and J. Shen. Error analysis of pressure-correction schemes for the time-dependent Stokes equations with open boundary conditions. *SIAM J. Numer. Anal.*, 43(1):239–258, 2005.

[19] J. L. Guermond, P. Minev, and J. Shen. An overview of projection methods for incompressible flows. *Comput. Methods Appl. Mech. Eng.*, 195(44-47):6011–6045, 2006.

[20] J. L. Guermond and J. Shen. A new class of truly consistent splitting schemes for incompressible flows. *J. Comput. Phys.*, 192(1):262–276, 2003.

[21] R. Haferssas, P. Jolivet, and S. Rubino. Efficient and scalable discretization of the Navier-Stokes equations with LPS modeling. *Comput. Methods Appl. Mech. Eng.*, 333:371–394, 2018.

[22] F. Hecht. New development in freefem++. *J. Numer. Math.*, 20(3-4):251–265, 2012.

[23] J. G. Heywood and R. Rannacher. Finite-element approximation of the nonstationary Navier-Stokes problem. IV: Error analysis for second-order time discretization. *SIAM J. Numer. Anal.*, 27(2):353–384, 1990.

[24] P. Holmes, J. L. Lumley, G. Berkooz, and C. W. Rowley. *Turbulence, coherent structures, dynamical systems and symmetry.* Camb. Monogr. Mech. Cambridge: Cambridge University Press, 2nd ed. edition, 2012.

[25] T. Iliescu and Z. Wang. Are the snapshot difference quotients needed in the proper orthogonal decomposition? *SIAM J. Sci. Comput.*, 36(3):a1221–a1250, 2014.

[26] T. Iliescu and Z. Wang. Variational multiscale proper orthogonal decomposition: Navier-Stokes equations. *Numer. Methods Partial Differ. Equations*, 30(2):641–663, 2014.

[27] A. Janes and J. R. Singler. A New Proper Orthogonal Decomposition Method with Second Difference Quotients for the Wave Equation. *Journal of Computational and Applied Mathematics*, 457:116279, 2025.

[28] K. Kean and M. Schneier. Error analysis of supremizer pressure recovery for POD based reduced-order models of the time-dependent Navier-Stokes equations. *SIAM J. Numer. Anal.*, 58(4):2235–2264, 2020.

[29] B. Koc, T. Chacón Rebollo, and S. Rubino. Uniform bounds with difference quotients for proper orthogonal decomposition reduced order models of the Burgers equation. *J. Sci. Comput.*, 95(2):27, 2023. Id/No 43.

[30] B. Koc, S. Rubino, M. Schneier, J. Singler, and T. Iliescu. On optimal pointwise in time error bounds and difference quotients for the proper orthogonal decomposition. *SIAM J. Numer. Anal.*, 59(4):2163–2196, 2021.

[31] K. Kunisch and S. Volkwein. Galerkin proper orthogonal decomposition methods for parabolic problems. *Numer. Math.*, 90(1):117–148, 2001.

[32] X. Li, Y. Luo, and M. Feng. An efficient Chorin-Temam projection proper orthogonal decomposition based reduced-order model for nonstationary Stokes equations. *J. Sci. Comput.*, 93(3):26, 2022. Id/No 64.

[33] B. R. Noack, P. Papas, and P. A. Monkewitz. The need for a pressure-term representation in empirical Galerkin models of incompressible shear flows. *J. Fluid Mech.*, 523:339–365, 2005.

[34] J. Novo and S. Rubino. Error analysis of proper orthogonal decomposition stabilized methods for incompressible flows. *SIAM J. Numer. Anal.*, 59(1):334–369, 2021.

[35] A. Poux, S. Glockner, and M. Azaïez. Improvements on open and traction boundary conditions for Navier-Stokes time-splitting methods. *J. Comput. Phys.*, 230(10):4011–4027, 2011.

[36] A. Quarteroni, F. Saleri, and A. Veneziani. Factorization methods for the numerical approximation of Navier-Stokes equations. *Comput. Methods Appl. Mech. Eng.*, 188(1-3):505–526, 2000.

[37] A. Quarteroni and A. Valli. *Numerical approximation of partial differential equations*, volume 23 of *Springer Ser. Comput. Math.* Berlin: Springer, 1994.

[38] S. Rubino. A streamline derivative POD-ROM for advection-diffusion-reaction equations. *ESAIM, Proc. Surv.*, 64:121–136, 2018.

[39] S. Rubino. An efficient time-splitting approximation of the Navier-Stokes equations with LPS modeling. *Appl. Math. Comput.*, 348:318–337, 2019.

[40] S. Rubino. Numerical analysis of a projection-based stabilized POD-ROM for incompressible flows. *SIAM J. Numer. Anal.*, 58(4):2019–2058, 2020.

[41] G. Stabile, S. Hijazi, A. Mola, S. Lorenzi, and G. Rozza. POD-Galerkin reduced order methods for CFD using finite volume discretisation: vortex shedding around a circular cylinder. *Commun. Appl. Ind. Math.*, 8(1):210–236, 2017.

[42] R. Témam. Sur l'approximation de la solution des équations de Navier-Stokes par la méthode des pas fractionnaires. II. *Arch. Ration. Mech. Anal.*, 33:377–385, 1969.